

Reconfigurable Intelligent Surface assisted Integrated Communication, Sensing, and Computation Systems

Jiahua Wan, Hong Ren, *Member, IEEE*, Zhiyuan Yu, Zhenkun Zhang, Yang Zhang, Cunhua Pan, *Senior Member, IEEE*, and Jiangzhou Wang, *Fellow, IEEE*

Abstract—This paper studies a mobile edge computing (MEC) assisted integrated sensing and communication (ISAC), where reconfigurable intelligent surface (RIS) is used to alleviate the attenuation of communication links during computational offloading. In this paradigm, the dual function radar and communication (DFRC)-enabled user equipments (UEs) simultaneously perform radar sensing and communication tasks, facilitating the offloading of partial computational tasks to an edge computing server (ECS) through an RIS. To satisfy the critical need for time-efficient sensing, we investigate the latency minimization problem for both single-UE and multi-UE scenarios, subject to constraints on UEs' transmit power, radar signal-to-interference-plus-noise-ratio (SINR), RIS phase shift, and computation capability. To address the formulated non-convex problem, we propose an algorithm based on the block coordinate descent (BCD) method to decouple the original problem into two subproblems, where the computational and beamforming settings are optimized alternately. Specifically, we employ the Lagrangian method for the optimization of computational settings. In addition, two equivalent transformations are applied to transform the objective function (OF) of the subproblem for active and passive beamforming into a form of weighted sum-rate. Then, a combination of minimum variance distortionless response (MVDR), successive convex approximation (SCA), majorization-minimization (MM), and weighted minimum mean-square error (WMMSE) techniques are applied to tackle this subproblem. Moreover, a closed-form solution is obtained in the simplified single UE scenario. Finally, simulation results substantiate the effectiveness of the proposed system.

Index Terms—Integrated communication, sensing, and computation (ICSC), dual function radar and communication (DFRC), reconfigurable intelligent surface (RIS), mobile edge computing (MEC)

I. INTRODUCTION

With the evolution of the sixth generation (6G) networks, the number of wireless communication user equipments (UEs) is exploding, leading to a scarcity of wireless spectrum resources [1]. Integrated sensing and communication (ISAC), emerging as a pivotal technology of 6G, concurrently fulfills communication and sensing functions by utilizing the same frequency band, thereby presenting an effective approach to improve spectral efficiency [2]–[4].

Part work of this article was accepted by the IEEE International Conference on Acoustics, Speech and Signal Processing Workshops (ICASSPW), Seoul, Korea, April 2024.

J. Wan, H. Ren, Z. Yu, Z. Zhang, Y. Zhang, and C. Pan are with National Mobile Communications Research Laboratory, Southeast University, Nanjing, China. (email: {wanjiahua, hren, zyyu, zhenkun_zhang, y_zhang, cpan}@seu.edu.cn). J. Wang is with the School of Engineering, University of Kent, Canterbury CT2 7NT, U.K. (e-mail: j.z.wang@kent.ac.uk).

Generally, ISAC can be classified into two principal research directions: radar and communication coexistence (RCC) and dual function radar communication (DFRC) systems [5]. In RCC, radar and communication subsystems typically operate independently, with research emphasis on mitigating interference through signal processing techniques such as interference cancellation, spatial separation, and precoding [6]. In contrast, DFRC techniques seamlessly merge radar sensing and wireless communications based on shared spectrum bands, hardware resources, and collaborative signal processing frameworks [7], [8]. Benefiting from this inherent integration, DFRC systems are more efficient for ISAC applications.

However, efficiently processing massive distributed ISAC data poses a significant challenge to the network. In conventional mobile cloud computing scenarios, the necessity to transfer sensing data and computation-intensive tasks to remote data centers for centralized processing often leads to high service latency and heavy traffic loads on core networks, primarily due to extended transmission distances. A promising solution for this issue emerges through the integration of mobile edge computing (MEC) [9] and ISAC. MEC facilitates the migration of computation capability to the wireless network edge by deploying edge servers at cellular base stations (BSs), as demonstrated in [10]. This strategic placement enables the execution of high computational tasks in proximity to ISAC application, thereby achieving ultra-low ISAC service latency while minimizing traffic loads. This innovative fusion of MEC with ISAC embodies the concept of integrated communication, sensing, and computation (ICSC) [11]–[14]. In this context, ICSC systems are commonly implemented in two primary paradigms: BS-centric and User-centric ICSC. In the BS-centric scheme, BSs are responsible for probing the sensing signal, while user equipments (UEs) are tasked with offloading the information to the BS [15]. However, in various ISAC application scenarios, such as vehicle-to-everything (V2X) networks [16], unmanned aerial vehicle (UAV) communication and sensing [17], and industrial internet of things (IoT) [18], UEs are required to sense the high mobility targets with low latency. This necessitates the exploration of User-centric ICSC systems, which aim to integrate the DFRC functionality into the ICSC framework. The User-centric ICSC scheme allows both sensing and communication tasks to leverage shared hardware platforms, enhancing the spectrum and energy efficiency. Recent contributions have focused on resource allocation in User-centric ICSC systems. A cooperative approach was in-

roduced in [19] to design radar sensing and communication waveforms, focusing on maximizing the energy efficiency of ICSC systems. The authors of [20] jointly optimized computational energy consumption and multi-input multi-output (MIMO) precoding for radar waveforms and communication symbols within ICSC systems, taking into account constraints related to latencies and resource limitations. Nonetheless, the efficacy of ICSC systems may be hindered in practical scenarios due to obstacles such as buildings and trees, which result in prolonged offloading delays in MEC [21] and diminished reception of sensing signals.

Fortunately, reconfigurable intelligent surface (RIS) shows promise in addressing the aforementioned challenges by enhancing channel quality through additional reliable links [22], [23]. On the one hand, existing contributions demonstrate that RIS is effective in reducing offloading latency in MEC systems for different scenarios [24]–[26]. Specifically, the authors of [24] designed an algorithm to minimize latency in MEC systems with the assistance of RIS in both single-UE and multi-UE scenarios. The contributions of [25] tackled a network-wide latency optimization problem in multi-RIS-assisted MEC systems. [26] focused on the issue of minimizing delays in RIS-assisted MEC systems where several end-users experience poor signal reception. On the other hand, recent studies have also shown the benefits of RIS in ISAC systems, where the RISs are employed to improve the quality of downlink communication and establish a reliable link between the transceiver and the target [27], [28]. In specific, the authors of [27] first introduced the utilization of RIS in a DFRC system to improve radar sensing performance, by optimizing the signal-to-noise ratio (SNR) at the radar receiver. Furthermore, the authors of [28] investigated the active RIS-aided ISAC systems to mitigate the four-hop multiplicative fading effect between the transceiver and the target.

The rapid development of the RIS-aided ISAC systems and the RIS-aided MEC systems has also inspired researchers to investigate the performance of the RIS-aided ICSC systems [29], [30]. In particular, [29] employed the RIS to alleviate the interference between radar and the edge computing server (ECS), and an energy-efficient system was proposed. The authors of [30] used the RIS as a passive information source in an ICSC system and introduced the weighted throughput capacity for performance evaluation. However, these studies only considered multi-input single-output (MISO) scenarios, which may not align with real-world engineering applications. More importantly, most of the contributions concentrated on the RIS-aided BS-centric ICSC, which cannot satisfy the increasing demands of processing large amounts of sensing data on the UE side.

Inspired by the preceding discussion, this paper delves into an investigation of the RIS-assisted User-centric ICSC system, where the RIS is deployed to facilitate the offloading of the computing data to the ECS. The main contributions of this paper are summarized as follows:

- An RIS-assisted ICSC system within a User-centric DFRC framework is investigated, where multiple DFRC-enabled UEs simultaneously detect targets and upload radar-sensing computational tasks to an ECS through

their communication functionalities. Specifically, we jointly optimize the precoding and decoding matrices of the uplink signal, the receive radar beamforming vector, the RIS phase shift vector, the offloading volume, and the edge computational resource allocation to minimize the weighted latency, with constraints on UEs' transmit power, radar signal-to-interference-plus-noise-ratio (SINR), RIS phase shift, and computation capability.

- A block coordinate descent (BCD)-based algorithm is proposed to effectively decouple the optimization of the computational settings and the active and passive beamforming matrices into two subproblems. The joint optimization of the offloading volume and edge computing resource allocation is addressed by applying Karush-Kuhn-Tucker (KKT) conditions and the bisection search method. Then, with fixed computing design, we deal with the joint optimization problem of passive and active beamforming, the objective function (OF) of which takes the form of a non-convex sum-of-ratios, presenting a significant challenge. To address this issue, the OF is transformed into a form of a weighted sum-rate through two equivalent transformations. Various algorithms such as the minimum variance distortionless response (MVDR), successive convex approximation (SCA), majorization-minimization (MM), and weighted minimum mean-square error (WMMSE) techniques are employed to solve the resulting problem.
- Furthermore, a specific scenario involving a single UE is examined, where the edge computational resource allocation and interference from multiple UEs are not considered. We derive a closed-form solution in each iteration.
- Simulation results verify the effectiveness of the proposed algorithms and the advantages of employing the RIS-assisted ICSC system.

Notation: Throughout this paper, scalars, vectors, and matrices are denoted by lowercase italicized letters, lowercase bold letters, and uppercase bold letters, respectively. $\mathbb{C}^{N \times M}$ denotes the space of $N \times M$ complex matrices. $(\cdot)^T$, $(\cdot)^*$, and $(\cdot)^H$ denote the transpose, complex conjugation, and Hermitian operators, respectively. $(\cdot)^*$ represents the optimal result of a variable. $\text{Tr}(\cdot)$ is the trace of a matrix. $\mathbb{E}(\cdot)$ denotes the statistical expectation operation. $\lfloor \cdot \rfloor$ and $\lceil \cdot \rceil$ are the floor and ceiling of a scalar, respectively. $\text{Re}\{\cdot\}$ and $\angle(\cdot)$ represent the real part and the argument of a complex number. \odot denotes the Hadamard product of two matrices. $\text{diag}\{\mathbf{x}\}$ means the diagonal matrix where the diagonal elements are \mathbf{x} . $|\cdot|$ and $\|\cdot\|$ represent the absolute value of a scalar and the Euclidean norm of a vector, respectively.

II. SYSTEM MODEL AND PROBLEM FORMULATION

A. Communication Model

Consider an RIS-assisted ICSC system as illustrated in Fig. 1, which consists of K DFRC-enabled UEs with N antennas, an L -element RIS, and an M -antenna BS connected to an ECS. Each UE is capable of simultaneously performing target sensing and offloading computational tasks to the BS through the communication link. Since UEs and their corresponding

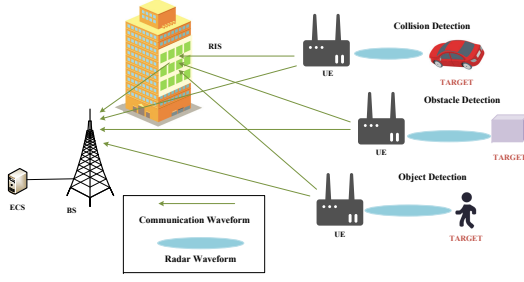


Fig. 1. System model.

targets are spatially separated from the BS, it is assumed that the RIS is dedicated to providing support for edge computing and does not impact the sensing capabilities of the UEs [31]. By defining the precoding matrix as $\mathbf{F}_{c,k} \in \mathbb{C}^{N \times d}$ and the transmit symbols as $\mathbf{c}_k = [c_{k,1}[n], \dots, c_{k,d}[n]]^T \in \mathbb{C}^{d \times 1}$, satisfying $\mathbb{E}[\mathbf{c}_k \mathbf{c}_k^H] = \mathbf{I}_d$ and $\mathbb{E}[\mathbf{c}_k \mathbf{c}_l^H] = \mathbf{0}_d$, the transmit signal of UE k is expressed as

$$\mathbf{x}_k = \mathbf{F}_{c,k} \mathbf{c}_k \in \mathbb{C}^{N \times 1}. \quad (1)$$

We denote the channels from UE k to the BS, from the RIS to the BS, and from UE k to the RIS by $\mathbf{H}_{\text{bu},k} \in \mathbb{C}^{M \times N}$, $\mathbf{H}_{\text{r}} \in \mathbb{C}^{M \times L}$, and $\mathbf{H}_{\text{ru},k} \in \mathbb{C}^{L \times N}$, respectively. For simplicity, the reflection elements of the RIS have unit amplitude and thus the reflecting coefficients matrix of the RIS can be expressed as $\mathbf{V} = \text{diag}\{e^{j\theta_1}, \dots, e^{j\theta_L}\} \in \mathbb{C}^{L \times L}$, where $\theta_l \in (0, 2\pi)$, $\forall l \in \mathcal{L} = \{1, \dots, L\}$ is the phase of the l -th reflecting element of RIS. The overall channel matrix between UE k and the BS is given by

$$\mathbf{H}_k \triangleq \mathbf{H}_{\text{bu},k} + \mathbf{H}_{\text{r}} \mathbf{V} \mathbf{H}_{\text{ru},k} \in \mathbb{C}^{M \times N}. \quad (2)$$

Then, the signal vector received at the BS is formulated as

$$\mathbf{y}_c = \sum_{k=1}^K \mathbf{H}_k \mathbf{F}_{c,k} \mathbf{c}_k + \mathbf{n}_c \in \mathbb{C}^{M \times 1}, \quad (3)$$

where $\mathbf{n}_c = [n_{c,1}, \dots, n_{c,M}]^T \in \mathbb{C}^{M \times 1} \sim \mathcal{CN}(\mathbf{0}, \sigma_c^2 \mathbf{I}_M)$ denotes the additive white Gaussian noise (AWGN) at the BS. After decoding the received signal with a linear matrix $\mathbf{W}_{c,k}$, we can obtain the recovered signal of UE k as

$$\begin{aligned} \hat{\mathbf{c}}_k &= \mathbf{W}_{c,k}^H \mathbf{y}_c \\ &= \mathbf{W}_{c,k}^H \left(\sum_{k=1}^K \mathbf{H}_k \mathbf{F}_{c,k} \mathbf{c}_k + \mathbf{n}_c \right) \in \mathbb{C}^{d \times 1}. \end{aligned} \quad (4)$$

The covariance of the transmit signal from UE k is given by

$$\mathbf{R}_{\mathbf{x},k} \triangleq \mathbb{E}[\mathbf{x}_k \mathbf{x}_k^H] = \mathbf{F}_{c,k} \mathbf{F}_{c,k}^H. \quad (5)$$

By denoting the transmit power of UE k by $P_{t,k}$, the power constraint for UE k is expressed as

$$\text{Tr}(\mathbf{R}_{\mathbf{x},k}) = \text{Tr}(\mathbf{F}_{c,k} \mathbf{F}_{c,k}^H) \leq P_{t,k}, \forall k \in \mathcal{K} = \{1, \dots, K\}. \quad (6)$$

Furthermore, the achievable off-loading rate (bit/s/Hz) of UE k can be formulated as

$$R_k(\mathbf{F}_c, \mathbf{W}_{c,k}, \boldsymbol{\theta}) \quad (7)$$

$$= B_\omega \log_2 |\mathbf{I}_d + \mathbf{W}_{c,k}^H \mathbf{H}_k \mathbf{F}_{c,k} \mathbf{F}_{c,k}^H \mathbf{H}_k^H \mathbf{W}_{c,k} (\mathbf{W}_{c,k}^H \mathbf{J}_k \mathbf{W}_{c,k})^{-1}|,$$

where B_ω denotes the bandwidth, and \mathbf{J}_k represents the interference plus noise matrix of UE k that is given by

$$\mathbf{J}_k = \sum_{i=1, i \neq k}^K \mathbf{H}_i \mathbf{F}_{c,i} \mathbf{F}_{c,i}^H \mathbf{H}_i^H + \sigma_c^2 \mathbf{I}_M \in \mathbb{C}^{M \times M}.$$

B. Radar Sensing Model

Given the transmit signal \mathbf{x}_k in (1), the received echo of UE k is expressed as

$$\mathbf{y}_{s,k} = \alpha_k \mathbf{a}_{\text{R},k}(\theta_k) \mathbf{a}_{\text{T},k}^H(\theta_k) \mathbf{x}_k + \sum_{i=1, i \neq k}^K \mathbf{H}_{k,i} \mathbf{x}_i + \mathbf{z}_k \in \mathbb{C}^{N \times 1}, \quad (8)$$

where α_k represents the amplitude of the radar target located at angle θ_k , $\mathbf{a}_{\text{R},k}(\theta_k) \in \mathbb{C}^{N \times 1}$ and $\mathbf{a}_{\text{T},k}(\theta_k) \in \mathbb{C}^{N \times 1}$ are the receive and transmit array response vectors for UE k , respectively. Matrix $\mathbf{H}_{k,i} \in \mathbb{C}^{N \times N}$ denotes the channel matrix between UE k and UE i , and $\mathbf{z}_k = [z_{k,1}, \dots, z_{k,N}]^T \in \mathbb{C}^{N \times 1}$ is the AWGN noise with the covariance of σ_s^2 . For simplicity, we define $\mathbf{G}_k \triangleq \alpha_k \mathbf{a}_{\text{R},k}(\theta_k) \mathbf{a}_{\text{T},k}^H(\theta_k) \in \mathbb{C}^{N \times N}$ as the target response matrix. Then, the radar output at UE k is given by

$$r_k = \mathbf{w}_{s,k}^H \mathbf{G}_k \mathbf{x}_k + \sum_{i=1, i \neq k}^K \mathbf{w}_{s,k}^H \mathbf{H}_{k,i} \mathbf{x}_i + \mathbf{w}_{s,k}^H \mathbf{z}_k, \quad (9)$$

where $\mathbf{w}_{s,k} \in \mathbb{C}^{N \times 1}$ is the receive beamforming vector of UE k .

The sensing performance can be measured in terms of the radar SINR. After applying receive beamforming, the radar SINR for UE k , denoted by γ_k , is given by

$$\begin{aligned} \gamma_k &= \frac{\mathbb{E} \left[|\mathbf{w}_{s,k}^H \mathbf{G}_k \mathbf{x}_k|^2 \right]}{\mathbb{E} \left[|\mathbf{w}_{s,k}^H (\sum_{i=1, i \neq k}^K \mathbf{H}_{k,i} \mathbf{x}_i + \mathbf{z}_k)|^2 \right]} \\ &= \frac{\text{Tr}(\mathbf{w}_{s,k}^H \mathbf{G}_k \mathbf{F}_{c,k} \mathbf{F}_{c,k}^H \mathbf{G}_k \mathbf{w}_{s,k})}{\text{Tr}(\mathbf{w}_{s,k}^H \mathbf{T}_k \mathbf{w}_{s,k})}, \end{aligned} \quad (10)$$

where $\mathbf{T}_k \triangleq \sum_{i=1, i \neq k}^K \mathbf{H}_{k,i} \mathbf{F}_{c,i} \mathbf{F}_{c,i}^H \mathbf{H}_{k,i}^H + \sigma_s^2 \mathbf{I}_N \in \mathbb{C}^{N \times N}$.

C. Computation Model

The partial off-loading strategy is adopted for computational tasks, where a fraction of the data is processed locally, while the remaining portion is offloaded to the BS.

a) *Local computation model*: For UE k , we denote V_k , v_k , c_k , and f_k^l by the overall number of bits awaiting processing, the number of bits designated for offloading, the number of CPU cycles required for processing each bit, and its CPU frequency, respectively. Then, the latency for local computation of UE k is given by $T_{1,k} = (V_k - v_k) c_k / f_k^l$.

b) *Edge computation model*: Let f_k^e with $\sum_{k=1}^K f_k^e \leq f_{\text{total}}^e$ denote the computation resources allocated to UE k , where f_{total}^e represents the processing rate of the ECS. It is assumed that the edge computing process for UE k begins when all v_k offloaded bits are received at the BS. The entire process of edge computation for UE k can be divided into

three steps: computing offloading, edge computing, and result feedback, with the feedback latency typically being neglected [32]. Consequently, the total latency of edge computation for UE k is expressed as $T_{c,k} = T_{o,k} + T_{e,k} = v_k/R_k(\mathbf{F}_c, \mathbf{W}_{c,k}, \boldsymbol{\theta}) + v_k c_k/f_k^e$.

We consider the simultaneous execution for local and edge computation. In this case, the latency of UE k can be represented by

$$\begin{aligned} T_k(\mathbf{F}_c, \mathbf{W}_{c,k}, \boldsymbol{\theta}, v_k, f_k^e) &= \max\{T_{1,k}, T_{c,k}\} \\ &= \max\left\{\frac{(V_k - v_k)c_k}{f_k^l}, \frac{v_k}{R_k(\mathbf{F}_c, \mathbf{W}_{c,k}, \boldsymbol{\theta})} + \frac{v_k c_k}{f_k^e}\right\}. \end{aligned} \quad (11)$$

D. Problem Formulation

In this paper, we aim to minimize the total weighted latency of all UEs by jointly optimizing the communication precoding matrices $\mathbf{F}_c = \{\mathbf{F}_{c,k}, \forall k \in \mathcal{K}\}$, the communication decoding matrices $\mathbf{W}_c = \{\mathbf{W}_{c,k}, \forall k \in \mathcal{K}\}$, the receive radar beamforming vectors $\mathbf{w}_s = \{\mathbf{w}_{s,k}, \forall k \in \mathcal{K}\}$, the RIS phase shift vector $\boldsymbol{\theta} = [\theta_1, \dots, \theta_L]$, the offloading volume $\mathbf{v} = [v_1, \dots, v_K]^T$, and the edge computational resource allocation $\mathbf{f} = [f_1^e, \dots, f_K^e]^T$. The optimization problem is formulated as

$$\mathcal{P}0: \min_{\mathbf{F}_c, \mathbf{W}_c, \mathbf{w}_s, \boldsymbol{\theta}, \mathbf{v}, \mathbf{f}} \sum_{k=1}^K \xi_k T_k(\mathbf{F}_c, \mathbf{W}_{c,k}, \boldsymbol{\theta}, v_k, f_k^e) \quad (12a)$$

$$s.t. \quad \text{Tr}(\mathbf{R}_{\mathbf{X},k}) \leq P_{t,k}, \forall k \in \mathcal{K}, \quad (12b)$$

$$\gamma_k \geq \eta, \forall k \in \mathcal{K}, \quad (12c)$$

$$0 < \theta_l \leq 2\pi, \forall l \in \mathcal{L}, \quad (12d)$$

$$\sum_{k=1}^K f_k^e \leq f_{\text{total}}^e, \quad (12e)$$

$$v_k \in \{0, 1, \dots, V_k\}, \forall k \in \mathcal{K}, \quad (12f)$$

$$f_k^e \geq 0, \forall k \in \mathcal{K}, \quad (12g)$$

where ξ_k represents the weight of UE k and η denotes the radar SINR requirement of UEs. The constraints (12e) - (12g) are introduced based on the computation model in Sec. II-C.

Addressing Problem $\mathcal{P}0$ poses several challenges. Firstly, the OF of Problem $\mathcal{P}0$ is in a segmented form. Secondly, the variables of Problem $\mathcal{P}0$ are highly coupled. Finally, the weighted total latency involves calculating the sum of ratios, which can often be challenging to optimize.

III. ALGORITHM DESIGN

In this section, Problem $\mathcal{P}0$ is decoupled into multiple sub-problems by using the BCD method, for which solutions are subsequently devised.

A. Joint Optimization of Offloading Volume \mathbf{v} and Edge Computing Resource Allocation \mathbf{f}

Given $\{\mathbf{F}_c, \mathbf{W}_c, \mathbf{w}_s, \boldsymbol{\theta}\}$, Problem $\mathcal{P}0$ is reformulated as

$$\begin{aligned} \mathcal{P}1: \min_{\mathbf{v}, \mathbf{f}} \quad & \sum_{k=1}^K \xi_k T_k(v_k, f_k^e) \\ s.t. \quad & (12e), (12f), (12g). \end{aligned} \quad (13)$$

It can be verified that $T_{1,k}$ and $T_{c,k}$ are respectively monotonically decreasing and increasing with respect to (w.r.t.) v_k . Therefore, given \mathbf{f} , the minimum value of $T_k(v_k) = \max\{T_{1,k}, T_{c,k}\}$ is obtained when $T_{1,k} = T_{c,k}$ is satisfied. Accordingly, the value of v_k that minimizes $T_k(v_k)$ without the integer constraint, denoted by \hat{v}_k^* , is given by

$$\hat{v}_k^* = \frac{V_k c_k R_k f_k^e}{f_k^e f_k^l + c_k R_k (f_k^e + f_k^l)}, \forall k \in \mathcal{K}. \quad (14)$$

Therefore, the optimal value of v_k is obtained according to

$$v_k^* = \arg \min_{v_k \in \{\lfloor \hat{v}_k^* \rfloor, \lceil \hat{v}_k^* \rceil\}} T_k(v_k), \forall k \in \mathcal{K}. \quad (15)$$

Given \mathbf{v} , Problem $\mathcal{P}1$ can be rewritten as follows:

$$\begin{aligned} \mathcal{P}1-1: \min_{\mathbf{f}} \quad & \sum_{k=1}^K \xi_k \frac{V_k c_k^2 R_k + L_k c_k f_k^e}{f_k^e f_k^l + c_k R_k (f_k^e + f_k^l)} \\ s.t. \quad & (12e), (12g). \end{aligned} \quad (16)$$

Problem $\mathcal{P}1-1$ is convex w.r.t. \mathbf{f} and satisfies the Slater's condition [33]. Hence, the optimal solution of Problem $\mathcal{P}1-1$ can be derived via the KKT conditions. Specifically, the Lagrangian function of Problem $\mathcal{P}1-1$ can be formulated as

$$\mathcal{L}(\mathbf{f}, \mu) = \sum_{k=1}^K \xi_k \frac{V_k c_k^2 R_k + L_k c_k f_k^e}{f_k^e f_k^l + c_k R_k (f_k^e + f_k^l)} + \mu \left(\sum_{k=1}^K f_k^e - f_{\text{total}}^e \right), \quad (17)$$

where $\mu \geq 0$ denotes the Lagrange multiplier. Furthermore, the KKT conditions for Problem 1-1 are expressed as

$$\frac{\partial \mathcal{L}}{\partial f_k^e} = \frac{-\xi V_k c_k^3 R_k^2}{[c_k R_k f_k^l + (f_k^l + c_k R_k) f_k^{e*}]^2 + \mu^*} = 0, \quad (18)$$

$$\mu^* \left(\sum_{k=1}^K f_k^{e*} - f_{\text{total}}^e \right) = 0, \quad (19)$$

$$f_k^{e*} \geq 0. \quad (20)$$

Given μ , we can obtain the value of f_k^{e*} by solving (18) as

$$f_k^{e*} = \sqrt{\frac{\xi V_k c_k^3 R_k^2}{\mu^*} - c_k R_k f_k^l}, \forall k \in \mathcal{K}. \quad (21)$$

From (20), we have $\sqrt{\frac{\xi V_k c_k^3 R_k^2}{\mu^*} - c_k R_k f_k^l} \geq 0$, and thus $\mu^* \leq \frac{\xi V_k c_k}{f_k^l}$. Consequently, the value μ^* is within the range of $(\mu_l, \mu_u) = (0, \min_k \frac{\xi V_k c_k}{f_k^l})$. As $\sum_{k=1}^K f_k^e$ monotonically decreases w.r.t. μ , the optimal solution for f_k^e can be obtained by performing the bisection search based on (19). The algorithm for solving Problem $\mathcal{P}1$ is outlined in Algorithm 1. The complexity of Algorithm 1 is mainly dependent on the bisection search method. Given the convergence criterion ϵ and the maximum iteration time for variables $\{\mathbf{v}, \mathbf{f}\}$, denoted by t_1^{\max} , the overall complexity of Algorithm 1 can be expressed as $\mathcal{O}(t_1^{\max} \log_2(\frac{\mu_u - \mu_l}{\epsilon}) K)$.

B. Joint Optimization of Passive and Active Beamforming $\{\mathbf{F}_c, \mathbf{W}_c, \mathbf{w}_s, \boldsymbol{\theta}\}$

1) *Problem Reformulation:* With the optimized offloading volume \mathbf{v} , minimizing T_k is equivalent to minimizing the

Algorithm 1 Joint optimization of $\{\mathbf{v}, \mathbf{f}\}$, given $\{\mathbf{F}_c, \mathbf{W}_c, \mathbf{w}_s, \boldsymbol{\theta}\}$

- 1: Initialize iteration number $t_1 = 0$. Set the maximum number of iterations to t_1^{\max} . Initialize \mathbf{f}^0 satisfying (12e) and (12g).
- 2: **Repeat**
- 3: Calculate $\mathbf{v}^{(t_1+1)}$ using (14).
- 4: Calculate μ and $\mathbf{f}^{(t_1+1)}$ accordingly using the bisection search method.
- 5: $t_1 \leftarrow t_1 + 1$.
- 6: **Until** $t_1 = t_1^{\max}$ **or**

$$\epsilon_1^{(t_1+1)} = \frac{|\text{obj}^{(t_1+1)}(\mathbf{v}, \mathbf{f}) - \text{obj}^{(t_1)}(\mathbf{v}, \mathbf{f})|}{\text{obj}^{(t_1+1)}(\mathbf{v}, \mathbf{f})} < \epsilon.$$

computing offloading latency. Therefore, given $\{\mathbf{v}, \mathbf{f}\}$, Problem $\mathcal{P}0$ is transformed into

$$\mathcal{P}2: \min_{\mathbf{F}_c, \mathbf{W}_c, \mathbf{w}_s, \boldsymbol{\theta}} \sum_{k=1}^K \xi_k \frac{v_k}{R_k(\mathbf{F}_c, \mathbf{W}_{c,k}, \boldsymbol{\theta})} \quad (22)$$

s.t. (12b), (12c), (12d).

The OF of Problem $\mathcal{P}2$ is in a non-convex sum-of-ratios form, thereby presenting challenges in devising solutions through the existing methods [34]. To address this issue, we first reformulate Problem $\mathcal{P}2$ by introducing an auxiliary variable $\boldsymbol{\lambda} = [\lambda_1, \dots, \lambda_K]$ as

$$\mathcal{P}2-1: \min_{\mathbf{F}_c, \mathbf{W}_c, \mathbf{w}_s, \boldsymbol{\theta}, \boldsymbol{\lambda}} \sum_{k=1}^K \lambda_k$$

s.t. $\frac{\xi_k v_k}{R_k(\mathbf{F}_c, \mathbf{W}_{c,k}, \boldsymbol{\theta})} \leq \lambda_k, \forall k \in \mathcal{K}$ (23)

(12b), (12c), (12d).

Then, we introduce the following proposition for further derivation.

Proposition 1. *If $\{\mathbf{F}_c^*, \mathbf{W}_c^*, \mathbf{w}_s^*, \boldsymbol{\theta}^*, \boldsymbol{\lambda}^*\}$ is the solution of Problem $\mathcal{P}2-1$, then $\boldsymbol{\delta}^* = [\delta_1^*, \dots, \delta_K^*]$ exists such that $\{\mathbf{F}_c^*, \mathbf{W}_c^*, \mathbf{w}_s^*, \boldsymbol{\theta}^*\}$ satisfies the KKT conditions of the following problem when $\boldsymbol{\lambda} = \boldsymbol{\lambda}^*$ and $\boldsymbol{\delta} = \boldsymbol{\delta}^*$*

$$\mathcal{P}2-2: \min_{\mathbf{F}_c, \mathbf{W}_c, \mathbf{w}_s, \boldsymbol{\theta}} \sum_{k=1}^K \delta_k [\xi_k v_k - \lambda_k R_k(\mathbf{F}_c, \mathbf{W}_{c,k}, \boldsymbol{\theta})] \quad (24)$$

s.t. (12b), (12c), (12d).

Furthermore, $\{\mathbf{F}_c^*, \mathbf{W}_c^*, \boldsymbol{\theta}^*\}$ satisfies the following equations when $\boldsymbol{\lambda} = \boldsymbol{\lambda}^*$ and $\boldsymbol{\delta} = \boldsymbol{\delta}^*$

$$\begin{cases} \delta_k^* = \frac{1}{R_k(\mathbf{F}_c^*, \mathbf{W}_{c,k}^*, \boldsymbol{\theta}^*)}, \forall k \in \mathcal{K}, \\ \lambda_k^* = \frac{\xi_k v_k}{R_k(\mathbf{F}_c^*, \mathbf{W}_{c,k}^*, \boldsymbol{\theta}^*)}, \forall k \in \mathcal{K}. \end{cases} \quad (25)$$

Proof. Please refer to Appendix A. \square

From Proposition 1, if $(\mathbf{F}_c^*, \mathbf{W}_c^*, \mathbf{w}_s^*, \boldsymbol{\theta}^*)$ is the solution to Problem $\mathcal{P}2-2$, and the value of $\boldsymbol{\lambda}$ and $\boldsymbol{\delta}$ are set following (25), then $(\mathbf{F}_c^*, \mathbf{W}_c^*, \mathbf{w}_s^*, \boldsymbol{\theta}^*, \boldsymbol{\lambda}^*)$ is the solution to Problem $\mathcal{P}2-1$. In the following, we propose an algorithm to solve Problem $\mathcal{P}2-3$

by alternately optimizing the sets $\{\boldsymbol{\lambda}, \boldsymbol{\delta}\}$ and $\{\mathbf{F}_c, \mathbf{W}_c, \mathbf{w}_s, \boldsymbol{\theta}\}$. Firstly, given $\{\mathbf{F}_c, \mathbf{W}_c, \mathbf{w}_s, \boldsymbol{\theta}\}$, $\boldsymbol{\lambda}$ and $\boldsymbol{\delta}$ are updated by using the modified Newton's method [24], [35]. Then, we optimize $\mathbf{F}_c, \mathbf{W}_c, \mathbf{w}_s$, and $\boldsymbol{\theta}$ given $\{\boldsymbol{\lambda}, \boldsymbol{\delta}\}$ according to Algorithm 3, which is discussed in the subsequent subsections. The procedure for solving Problem $\mathcal{P}2-2$ is summarized in Algorithm 2, where we have

$$\chi_k(\delta_k) = \delta_k R_k(\mathbf{F}_c^*, \mathbf{W}_{c,k}^*, \boldsymbol{\theta}^*) - 1, \forall k \in \mathcal{K}, \quad (26)$$

$$\kappa_k(\lambda_k) = \lambda_k R_k(\mathbf{F}_c^*, \mathbf{W}_{c,k}^*, \boldsymbol{\theta}^*) - \xi_k v_k, \forall k \in \mathcal{K}. \quad (27)$$

Algorithm 2 Joint optimization of $\{\mathbf{F}_c, \mathbf{W}_c, \mathbf{w}_s, \boldsymbol{\theta}\}$, given $\{\mathbf{v}, \mathbf{f}\}$.

- 1: Initialize iteration number $t_2 = 0$ and step $\zeta \in (0, 1)$. Set the maximum number of iterations to t_2^{\max} . Calculate $R_k^{(0)}$ using (35), $\boldsymbol{\delta}^{(0)}$ and $\boldsymbol{\lambda}^{(0)}$ using (25).
- 2: **Repeat**
- 3: Calculate $\{\mathbf{F}_c^{(t_2+1)}, \mathbf{W}_c^{(t_2+1)}, \mathbf{w}_s^{(t_2+1)}, \boldsymbol{\theta}^{(t_2+1)}\}$ using Algorithm 3.
- 4: Update $\delta_k^{(t_2+1)}$ and $\lambda_k^{(t_2+1)}$ by

$$\delta_k^{(t_2+1)} = \delta_k^{(t_2)} - \frac{\zeta^i \chi_k(\delta_k^{(t_2)})}{R_k^{(t_2+1)}(\mathbf{F}_c, \mathbf{W}_c, \boldsymbol{\theta})}, \quad (28)$$

$$\lambda_k^{(t_2+1)} = \lambda_k^{(t_2)} - \frac{\zeta^i \kappa_k(\lambda_k^{(t_2)})}{R_k^{(t_2+1)}(\mathbf{F}_c, \mathbf{W}_c, \boldsymbol{\theta})}, \quad (29)$$

where $i^{(t_2+1)}$ is the smallest integer satisfying

$$\begin{aligned} & \sum_{k=1}^K \left| \chi_k \left(\delta_k^{(t_2)} - \frac{\zeta^i \chi_k(\delta_k^{(t_2)})}{R_k^{(t_2+1)}(\mathbf{F}_c, \mathbf{W}_c, \boldsymbol{\theta})} \right) \right|^2 + \\ & \sum_{k=1}^K \left| \kappa_k \left(\lambda_k^{(t_2)} - \frac{\zeta^i \kappa_k(\lambda_k^{(t_2)})}{R_k^{(t_2+1)}(\mathbf{F}_c, \mathbf{W}_c, \boldsymbol{\theta})} \right) \right|^2 \\ & \leq (1 - \epsilon_3 \zeta^i)^2 \sum_{k=1}^K \left[\left| \chi_k(\delta_k^{(t_2+1)}) \right|^2 + \left| \kappa_k(\lambda_k^{(t_2+1)}) \right|^2 \right]. \end{aligned} \quad (30)$$

- 5: $t_2 \leftarrow t_2 + 1$.
 - 6: **Until** $\chi_k(\delta_k^{(t_2)}) = 0$ and $\kappa_k(\lambda_k^{(t_2)}) = 0$ **or** $t_2 = t_2^{\max}$.
-

2) *Joint active and passive Beamforming Optimization:* In this case, Problem $\mathcal{P}2-2$ can be transformed into

$$\mathcal{P}2-3: \max_{\mathbf{F}_c, \mathbf{W}_c, \mathbf{w}_s, \boldsymbol{\theta}} \sum_{k=1}^K \delta_k \lambda_k R_k(\mathbf{F}_c, \mathbf{W}_{c,k}, \boldsymbol{\theta}) \quad (31)$$

s.t. (12b), (12c), (12d).

a) *OF Reformulation and decoding matrix design:* By introducing an auxiliary matrix \mathbf{D}_k , the equivalent formulation of Problem $\mathcal{P}2-3$ with constants removed can be derived as [36]

$$\mathcal{P}2-4: \min_{\mathbf{F}_c, \mathbf{W}_c, \mathbf{w}_s, \boldsymbol{\theta}, \mathbf{D}} \sum_{k=1}^K \delta_k \lambda_k \text{Tr}(\mathbf{D}_k \mathbf{E}_k(\mathbf{F}_c, \mathbf{W}_{c,k}, \boldsymbol{\theta}))$$

$-\delta_k \lambda_k \log_2 |\mathbf{D}_k|$ (32)

s.t. (12b), (12c), (12d),

where $\mathbf{D} = \{\mathbf{D}_k, \forall k \in \mathcal{K}\}$ and $\mathbf{E}_k(\mathbf{F}_c, \mathbf{W}_{c,k}, \boldsymbol{\theta}) \in \mathbb{C}^{d \times d}$ is the mean-square error (MSE) matrix of UE k given by

$$\begin{aligned} \mathbf{E}_k(\mathbf{F}_c, \mathbf{W}_{c,k}, \boldsymbol{\theta}) &= \mathbb{E}[(\hat{\mathbf{c}}_k - \mathbf{c}_k)(\hat{\mathbf{c}}_k - \mathbf{c}_k)^H] \\ &= (\mathbf{W}_{c,k}^H \mathbf{H}_k \mathbf{F}_{c,k} - \mathbf{I})(\mathbf{W}_{c,k}^H \mathbf{H}_k \mathbf{F}_{c,k} - \mathbf{I})^H \\ &+ \sum_{i=1, i \neq k}^K \mathbf{W}_{c,k}^H \mathbf{H}_i \mathbf{F}_{c,i} \mathbf{F}_{c,i}^H \mathbf{H}_i^H \mathbf{W}_{c,k} + \sigma_c^2 \mathbf{W}_{c,k}^H \mathbf{W}_{c,k}. \end{aligned}$$

In the following, we design an algorithm for solving Problem $\mathcal{P}2-4$ by alternately optimizing the beamforming variables $\{\mathbf{F}_c, \mathbf{W}_c, \mathbf{w}_s, \boldsymbol{\theta}\}$ under the BCD framework. Given $\{\mathbf{F}_c, \mathbf{w}_s, \boldsymbol{\theta}\}$, Problem $\mathcal{P}2-4$ is marginal convex w.r.t. $\{\mathbf{W}_c, \mathbf{D}\}$. Hence, by setting the first-order derivative of the OF of Problem $\mathcal{P}2-4$ w.r.t. $\mathbf{W}_{c,k}$ and \mathbf{D}_k to zero, respectively, the optimal solutions are obtained as

$$\mathbf{W}_{c,k}^* = (\mathbf{J}_k + \mathbf{H}_k \mathbf{F}_{c,k} \mathbf{F}_{c,k}^H \mathbf{H}_k^H)^{-1} \mathbf{H}_k \mathbf{F}_{c,k}, \quad (33)$$

$$\mathbf{D}_k^* = (\mathbf{E}_k^{(\text{MMSE})})^{-1}, \quad (34)$$

where

$$\mathbf{E}_k^{(\text{MMSE})} = \mathbf{I}_d - \mathbf{F}_{c,k}^H \mathbf{H}_k^H (\mathbf{J}_k + \mathbf{H}_k \mathbf{F}_{c,k} \mathbf{F}_{c,k}^H \mathbf{H}_k^H)^{-1} \mathbf{H}_k \mathbf{F}_{c,k}$$

is the minimum mean square error (MMSE) of UE k .

Meanwhile, R_k is given by

$$R_k = B_\omega \log_2 |(\mathbf{E}_k^{(\text{MMSE})})^{-1}|. \quad (35)$$

b) Receive and Transmit Beamforming Design for the UE: We first consider the optimization of the receive beamforming vector of UE k $\mathbf{w}_{s,k}$ with a fixed \mathbf{F}_c . Note that $\mathbf{w}_{s,k}$ is only related to the radar SINR constraint (12c). The optimal $\mathbf{w}_{s,k}$ that maximizes the sensing SINR is given by

$$\mathbf{w}_{s,k}^* = \arg \max_{\mathbf{w}_{s,k}} \frac{\mathbf{w}_{s,k}^H \mathbf{G}_k \mathbf{F}_{c,k} \mathbf{F}_{c,k}^H \mathbf{G}_k^H \mathbf{w}_{s,k}}{\mathbf{w}_{s,k}^H \mathbf{T}_k \mathbf{w}_{s,k}}, \quad (36)$$

which equals the eigenvector corresponding to the largest generalized eigenvalue of the matrix $[\mathbf{T}_k^{-1} \mathbf{G}_k \mathbf{F}_{c,k} \mathbf{F}_{c,k}^H \mathbf{G}_k^H]$ according to the MVDR method [37].

In the following, we focus on optimizing the transmit beamforming matrices \mathbf{F}_c with the fixed $\mathbf{w}_{s,k}$. First, the non-convex fractional inequalities (12c) can be rewritten as

$$\eta \text{Tr}(\mathbf{T}_k \mathbf{w}_{s,k} \mathbf{w}_{s,k}^H) - \text{Tr}(\mathbf{G}_k \mathbf{F}_{c,k} \mathbf{F}_{c,k}^H \mathbf{G}_k^H \mathbf{w}_{s,k} \mathbf{w}_{s,k}^H) \leq 0, \forall k \in \mathcal{K}, \quad (37)$$

where the SCA method can be applied to derive a convex upper bound of (37). By defining $f(\mathbf{F}_c) \triangleq -\text{Tr}(\mathbf{G}_k \mathbf{F}_{c,k} \mathbf{F}_{c,k}^H \mathbf{G}_k^H \mathbf{w}_{s,k} \mathbf{w}_{s,k}^H)$, the first-order Taylor approximation of $f(\mathbf{F}_c)$ at $\mathbf{F}_c^{(t)}$ in the t -th iteration can be formulated as

$$\begin{aligned} f(\mathbf{F}_c, \mathbf{F}_c^{(t)}) &= \text{Tr}(\mathbf{G}_k^T \mathbf{w}_{s,k}^* \mathbf{w}_{s,k}^{*T} \mathbf{G}_k^* \mathbf{F}_{c,k}^{(t)*} \mathbf{F}_{c,k}^{(t)*T}) \\ &- 2\text{Re}\{\text{Tr}(\mathbf{G}_k^H \mathbf{w}_{s,k} \mathbf{w}_{s,k}^H \mathbf{G}_k \mathbf{F}_{c,k} \mathbf{F}_{c,k}^{(t)*H})\}. \end{aligned} \quad (38)$$

Then, with $\{\mathbf{W}_c, \mathbf{w}_s, \boldsymbol{\theta}, \mathbf{D}\}$ fixed, Problem $\mathcal{P}2-4$ can be approximated as

$$\begin{aligned} \mathcal{P}2-5: \min_{\mathbf{F}_c} & \sum_{k=1}^K \sum_{i=1}^K \delta_k \lambda_k \text{Tr}(\mathbf{D}_k \mathbf{W}_{c,k}^H \mathbf{H}_i \mathbf{F}_{c,i} \mathbf{F}_{c,i}^H \mathbf{H}_i^H \mathbf{W}_{c,k}) - \\ & \sum_{k=1}^K \delta_k \lambda_k \text{Tr}(\mathbf{D}_k (\mathbf{F}_{c,k}^H \mathbf{H}_k^H \mathbf{W}_{c,k} + \mathbf{W}_{c,k}^H \mathbf{H}_k \mathbf{F}_{c,k})) \end{aligned}$$

$$\text{s.t. } \text{Tr}(\mathbf{R}_{\mathbf{X},k}) \leq P_{t,k}, \forall k \in \mathcal{K}, \quad (39)$$

$$\eta \text{Tr}(\mathbf{T}_k \mathbf{w}_{s,k} \mathbf{w}_{s,k}^H) + f(\mathbf{F}_c, \mathbf{F}_c^{(t)}) \leq 0, \forall k \in \mathcal{K}.$$

It can be verified that Problem $\mathcal{P}2-5$ is a convex problem, which can be efficiently solved via CVX [38].

c) RIS Phase Shift Design: Finally, we focus on the optimization of the phase shift of the RIS $\boldsymbol{\theta}$. The corresponding subproblem can be formulated as

$$\begin{aligned} \mathcal{P}2-6: \min_{\boldsymbol{\theta}} & \sum_{k=1}^K \sum_{i=1}^K \delta_k \lambda_k \text{Tr}(\mathbf{D}_k \mathbf{W}_{c,k}^H \mathbf{H}_i \mathbf{F}_{c,i} \mathbf{F}_{c,i}^H \mathbf{H}_i^H \mathbf{W}_{c,k}) - \\ & \sum_{k=1}^K \delta_k \lambda_k \text{Tr}(\mathbf{D}_k (\mathbf{F}_{c,k}^H \mathbf{H}_k^H \mathbf{W}_{c,k} + \mathbf{W}_{c,k}^H \mathbf{H}_k \mathbf{F}_{c,k})) \\ \text{s.t. } & 0 < \theta_l \leq 2\pi, \forall l \in \mathcal{L}. \end{aligned} \quad (40)$$

By defining $\mathbf{H}_k \triangleq \mathbf{H}_{\text{bu},k} + \mathbf{H}_r \mathbf{V} \mathbf{H}_{\text{ru},k}$, we have

$$\begin{aligned} \mathbf{D}_k \mathbf{W}_{c,k}^H \mathbf{H}_i \mathbf{F}_{c,i} \mathbf{F}_{c,i}^H \mathbf{H}_i^H \mathbf{W}_{c,k} &= \mathbf{D}_k \mathbf{W}_{c,k}^H \mathbf{H}_{\text{bu},i} \mathbf{F}_{c,i} \mathbf{F}_{c,i}^H \mathbf{H}_{\text{ru},i}^H \mathbf{V}^H \mathbf{H}_r^H \mathbf{W}_{c,k} \\ &+ \mathbf{D}_k \mathbf{W}_{c,k}^H \mathbf{H}_r \mathbf{V} \mathbf{H}_{\text{ru},i} \mathbf{F}_{c,i} \mathbf{F}_{c,i}^H \mathbf{H}_{\text{bu},i}^H \mathbf{W}_{c,k} \\ &+ \mathbf{D}_k \mathbf{W}_{c,k}^H \mathbf{H}_r \mathbf{V} \mathbf{H}_{\text{ru},i} \mathbf{F}_{c,i} \mathbf{F}_{c,i}^H \mathbf{H}_{\text{ru},i}^H \mathbf{V}^H \mathbf{H}_r^H \mathbf{W}_{c,k} \\ &+ \mathbf{D}_k \mathbf{W}_{c,k}^H \mathbf{H}_{\text{bu},i} \mathbf{F}_{c,i} \mathbf{F}_{c,i}^H \mathbf{H}_{\text{bu},i}^H \mathbf{W}_{c,k}, \end{aligned} \quad (41)$$

and

$$\begin{aligned} \mathbf{D}_k (\mathbf{F}_{c,k}^H \mathbf{H}_k^H \mathbf{W}_{c,k} + \mathbf{W}_{c,k}^H \mathbf{H}_k \mathbf{F}_{c,k}) &= \mathbf{D}_k \mathbf{F}_{c,k}^H \mathbf{H}_{\text{ru},k}^H \mathbf{V}^H \mathbf{H}_r^H \mathbf{W}_{c,k} + \mathbf{D}_k \mathbf{F}_{c,k}^H \mathbf{H}_{\text{bu},k}^H \mathbf{W}_{c,k} \\ &+ \mathbf{D}_k \mathbf{W}_{c,k}^H \mathbf{H}_r \mathbf{V} \mathbf{H}_{\text{ru},k} \mathbf{F}_{c,k} + \mathbf{D}_k \mathbf{W}_{c,k}^H \mathbf{H}_{\text{bu},k} \mathbf{F}_{c,k}. \end{aligned} \quad (42)$$

By defining $\mathbf{S}_{k,i} \triangleq \mathbf{H}_r^H \mathbf{W}_{c,k} \mathbf{D}_k \mathbf{W}_{c,k}^H \mathbf{H}_{\text{bu},i} \mathbf{F}_{c,i} \mathbf{F}_{c,i}^H \mathbf{H}_{\text{ru},i}^H$, $\mathbf{B}_i \triangleq \mathbf{H}_{\text{ru},i} \mathbf{F}_{c,i} \mathbf{F}_{c,i}^H \mathbf{H}_{\text{ru},i}^H$, $\mathbf{C}_k \triangleq \mathbf{H}_r^H \mathbf{W}_{c,k} \mathbf{D}_k \mathbf{W}_{c,k}^H \mathbf{H}_r$, and $\mathbf{P}_{k,i} \triangleq \mathbf{H}_{\text{ru},i} \mathbf{F}_{c,i} \mathbf{D}_k \mathbf{W}_{c,k}^H \mathbf{H}_r$, (41) and (42) are further transformed to

$$\begin{aligned} \text{Tr}(\mathbf{D}_k \mathbf{W}_{c,k}^H \mathbf{H}_i \mathbf{F}_{c,i} \mathbf{F}_{c,i}^H \mathbf{H}_i^H \mathbf{W}_{c,k}) &= \text{Tr}(\mathbf{V} \mathbf{B}_i \mathbf{V}^H \mathbf{C}_k) + \text{Tr}(\mathbf{V}^H \mathbf{S}_{k,i}) + \text{Tr}(\mathbf{V} \mathbf{S}_{k,i}^H) + \text{const}_1, \end{aligned} \quad (43)$$

and

$$\begin{aligned} \text{Tr}(\mathbf{D}_k (\mathbf{F}_{c,k}^H \mathbf{H}_k^H \mathbf{W}_{c,k} + \mathbf{W}_{c,k}^H \mathbf{H}_k \mathbf{F}_{c,k})) &= \text{Tr}(\mathbf{P}_{k,i} \mathbf{V}) + \text{Tr}(\mathbf{P}_{k,i}^H \mathbf{V}^H) + \text{const}_2, \end{aligned} \quad (44)$$

where const_1 and const_2 are constant independent of \mathbf{V} . Thus, Problem $\mathcal{P}2-6$ can be rewritten as

$$\begin{aligned} \mathcal{P}2-7: \min_{\boldsymbol{\theta}} & \text{Tr}(\mathbf{V} \mathbf{B} \mathbf{V}^H \mathbf{C}) + \text{Tr}(\mathbf{V} \mathbf{U}) + \text{Tr}(\mathbf{V}^H \mathbf{U}^H) \\ \text{s.t. } & 0 < \theta_l \leq 2\pi, \forall l \in \mathcal{L}, \end{aligned} \quad (45)$$

where $\mathbf{B} \triangleq \sum_{i=1}^K \mathbf{B}_i$, $\mathbf{C} \triangleq \sum_{k=1}^K \delta_k \lambda_k \mathbf{C}_k$, and $\mathbf{U} \triangleq \sum_{i=1}^K \sum_{k=1}^K \delta_k \lambda_k (\mathbf{S}_{k,i}^H - \mathbf{P}_{k,i})$.

With the definitions of $\boldsymbol{\phi} \triangleq [e^{j\theta_1}, \dots, e^{j\theta_L}]^T$ and $\mathbf{u} = [[\mathbf{U}]_{1,1}, \dots, [\mathbf{U}]_{L,L}]^T$, we have

$$\text{Tr}(\mathbf{V} \mathbf{B} \mathbf{V}^H \mathbf{C}) = \boldsymbol{\phi}^H (\mathbf{C} \odot \mathbf{B}^T) \boldsymbol{\phi}, \quad (46)$$

and

$$\text{Tr}(\mathbf{V} \mathbf{U}) = \boldsymbol{\phi}^T \mathbf{u}, \text{Tr}(\mathbf{V}^H \mathbf{U}^H) = \mathbf{u}^H \boldsymbol{\phi}^*. \quad (47)$$

Accordingly, Problem $\mathcal{P}2-7$ can be reformulated as

$$\begin{aligned} \mathcal{P}2-8: \min_{\boldsymbol{\phi}} & g(\boldsymbol{\phi}) = \boldsymbol{\phi}^H \boldsymbol{\Xi} \boldsymbol{\phi} + 2\text{Re}\{\boldsymbol{\phi}^H \mathbf{u}^*\} \\ \text{s.t. } & |\phi_l| = 1, \forall l \in \mathcal{L}, \end{aligned} \quad (48)$$

where $\Xi \triangleq \mathbf{C} \odot \mathbf{B}^T$. Problem $\mathcal{P}2-8$ is a non-convex problem owing to the unit modulus constraint. In the following, the MM algorithm [39] with two steps is applied to tackle this problem. Specifically, the surrogate function $h(\phi|\phi^{(t)})$ at the t -th iteration $\phi^{(t)}$, is introduced in the majorization step to provide an upper bound for $g(\phi)$. Then, in the minimization step, we update ϕ by $\phi^{(t+1)} \in \arg \min_{\phi} h(\phi|\phi^{(t)})$. To this end, we introduce the lemma below to construct the surrogate function of $g(\phi)$.

Lemma 1. *By denoting the maximum eigenvalue of Ξ by λ_{\max} , we have*

$$g(\phi) \leq \phi^H \lambda_{\max} \mathbf{I}_L \phi - 2\text{Re}\{\phi^H (\lambda_{\max} \mathbf{I}_L - \Xi) \phi^{(t)}\} + \phi^{(t)H} (\lambda_{\max} \mathbf{I}_L - \Xi) \phi^{(t)} + 2\text{Re}\{\phi^H \mathbf{u}^*\} \triangleq h(\phi|\phi^{(t)}). \quad (49)$$

Proof. Please refer to [39], [40]. \square

Note that $\phi^H \phi = L$, $\phi^H \lambda_{\max} \mathbf{I}_L \phi = L \lambda_{\max}$ is a constant. Thus, with constants independent of ϕ removed, Problem $\mathcal{P}2-8$ with the surrogate function at the $t+1$ -th iteration can be formulated as

$$\begin{aligned} \mathcal{P}2-9: \max_{\phi} \quad & \text{Re}\{\phi^H [(\lambda_{\max} \mathbf{I}_L - \Xi) \phi^{(t)} - \mathbf{u}^*]\} \\ \text{s.t.} \quad & |\phi_l| = 1, \forall l \in \mathcal{L}. \end{aligned} \quad (50)$$

Thus, the optimal solution for θ t the $t+1$ -th iteration is given by

$$\theta^{(t+1)} = \angle((\lambda_{\max} \mathbf{I}_L - \Xi) \phi^{(t)} - \mathbf{u}^*). \quad (51)$$

According to the preceding analysis, the procedure for solving Problem $\mathcal{P}2-4$ is summarized in Algorithm 3. The complexity of this algorithm is provided as follows. Since the number of variables in Step 3 is KNd , the complexity of updating $\mathbf{F}_c^{(t_3+1)}$ via the SCA method is given by $\mathcal{O}((KNd)^{3.5})$. In Step 4, the complexities of calculating $\mathbf{W}_c^{(t_3+1)}$ and $\mathbf{D}^{(t_3+1)}$ are on the order of $\mathcal{O}(KM^3)$ and $\mathcal{O}(Kd^3)$, respectively. In Step 5, the complexity of calculating $\mathbf{w}_s^{(t_3+1)}$ is $\mathcal{O}(KN^3)$. Defining the number of iterations as t_{MM}^{\max} , the computation complexity of updating $\theta^{(t_3+1)}$ via the MM algorithm in Step 6 contains two parts. Specifically, the complexity of calculating the maximum eigenvalue λ_{\max} of Ξ is on the order of $\mathcal{O}(L^3)$. Note that the main complexity for each iteration of the MM algorithm arises from calculating $\phi^{(t)}$, whose complexity is given by $\mathcal{O}(L^2)$. Hence, the total complexity of updating $\theta^{(t_3+1)}$ is on the order of $\mathcal{O}(L^3 + t_{MM}^{\max} L^2)$. By aggregating these components, the overall complexity of Algorithm 3 is given by $\mathcal{O}(t_3^{\max} \cdot \max\{(KNd)^{3.5}, KM^3, Kd^3, KN^3, L^3 + t_{MM}^{\max} L^2\})$. Furthermore, the complexity of Algorithm 2 is dominated by calculating $\{\mathbf{F}_c^{(t_2+1)}, \mathbf{W}_c^{(t_2+1)}, \mathbf{w}_s^{(t_2+1)}, \theta^{(t_2+1)}\}$ using Algorithm 3, as all other steps involve explicit closed-form solutions.

C. Summarize of the Algorithm Development

Following the above discussions, we present the overall BCD algorithm for solving Problem $\mathcal{P}0$ in Algorithm 4. The monotonic increase in the OF value of Problem $\mathcal{P}0$ at each step of Algorithm 4 is readily verified. Furthermore, the edge computing resource constraints impose an upper bound on the

Algorithm 3 Joint optimization of $\{\mathbf{F}_c, \mathbf{W}_c, \mathbf{w}_s, \theta\}$, Given $\{\delta, \lambda\}$.

- 1: Initialize iteration number $t_3 = 0$. Set the maximum number of iterations to t_3^{\max} . Initialize feasible $\mathbf{F}_c^{(0)}$, $\mathbf{w}_s^{(0)}$ and $\theta^{(0)}$ following constraints (12b) - (12d). Calculate $R_k^{(0)}$ using (35).
- 2: **Repeat**
- 3: Update $\mathbf{F}_c^{(t_3+1)}$ by solving Problem 2-5 with the SCA method.
- 4: Calculate $\mathbf{W}_c^{(t_3+1)}$ and $\mathbf{D}^{(t_3+1)}$ according to (33) and (34), respectively.
- 5: Calculate $\mathbf{w}_s^{(t_3+1)}$ by using (36).
- 6: Update $\theta^{(t_3+1)}$ using MM algorithm.
- 7: $t_3 \leftarrow t_3 + 1$.
- 8: **Until** $t_3 = t_3^{\max}$ **or**

$$\epsilon_3^{(t_1+1)} = \frac{|\text{obj}^{(t_3+1)}(\mathbf{F}_c, \theta) - \text{obj}^{(t_3)}(\mathbf{F}_c, \theta)|}{\text{obj}^{(t_3+1)}(\mathbf{F}_c, \theta)} < \epsilon.$$

OF value. Hence, Algorithm 4 is guaranteed to converge. The complexity of Algorithm 4 is mainly determined by Step 3 and Step 4, the complexities of which have been thoroughly discussed in the preceding subsections.

IV. SPECIFIC CASE STUDY

A special case with a single UE that transmits a single data stream is studied in this section to explore more insights. Here, we assume that the number of the data streams d is 1. The radar SINR constraint (12c) degenerates to the SNR constraint. Furthermore, since there is no need for the consideration of edge computing resource allocation, the sum-of-ratios form in the OF of Problem $\mathcal{P}2$ is transformed into a single-ratio form. In this instance, Problem $\mathcal{P}0$ is simplified as follows:

$$\mathcal{P}3: \min_{\mathbf{f}_c, \mathbf{w}_c, \mathbf{w}_s, \theta, v} T(\mathbf{f}_c, \mathbf{w}_c, \theta, v) \quad (52a)$$

$$\text{s.t.} \quad \text{Tr}(\mathbf{R}_x) \leq P_t, \quad (52b)$$

$$\gamma \geq \eta, \quad (52c)$$

$$0 < \theta_l \leq 2\pi, \forall l \in \mathcal{L}, \quad (52d)$$

$$v \in \{0, 1, \dots, V\}. \quad (52e)$$

Algorithm 4 Joint optimization of $\mathbf{v}, \mathbf{f}, \mathbf{F}_c$ and θ .

- 1: Initialize iteration number $t_4 = 0$. Set the maximum number of iterations to t_4^{\max} . Initialize feasible $\mathbf{f}^{(0)}$, $\mathbf{F}_c^{(0)}$, $\mathbf{w}_s^{(0)}$ and $\theta^{(0)}$ following constraints (12b) - (12e) and (12g).
- 2: **Repeat**
- 3: Calculate $\mathbf{v}^{(t_4+1)}$ and $\mathbf{f}^{(t_4+1)}$ via Algorithm 1.
- 4: Calculate $\mathbf{F}_c^{(t_4+1)}$, $\mathbf{W}_c^{(t_4+1)}$, $\mathbf{w}_s^{(t_4+1)}$ and $\theta^{(t_4+1)}$ via Algorithm 2.
- 5: $t_4 \leftarrow t_4 + 1$.
- 6: **Until** $t_4 = t_4^{\max}$ **or**

$$\epsilon_4^{(t_1+1)} = \frac{|\text{obj}^{(t_4+1)}(\mathbf{v}, \mathbf{f}, \mathbf{F}_c, \theta) - \text{obj}^{(t_4)}(\mathbf{v}, \mathbf{f}, \mathbf{F}_c, \theta)|}{\text{obj}^{(t_4+1)}(\mathbf{v}, \mathbf{f}, \mathbf{F}_c, \theta)} < \epsilon.$$

where η represents the SNR threshold of the UE for radar sensing, $\mathbf{f}_c \in \mathbb{C}^{N \times 1}$ and $\mathbf{w}_c \in \mathbb{C}^{M \times 1}$ denote the precoding and decoding vectors, respectively.

The BCD method is employed to solve Problem $\mathcal{P}3$. As discussed in Sec. III-A, given $\{\mathbf{f}_c, \mathbf{w}_c, \mathbf{w}_s, \boldsymbol{\theta}\}$, the optimal solution for v is obtained when $T_1 = T_c$. Consequently, the optimal v is equal to

$$v^* = \arg \min_{\hat{v} \in \{[\hat{v}^*], [\hat{v}^*]\}} T(\hat{v}), \quad (53)$$

where

$$\hat{v}^* = \frac{VcRf_{\text{total}}^e}{f_{\text{total}}^e f^l + cR(f_{\text{total}}^e + f^l)}. \quad (54)$$

Given v , Problem $\mathcal{P}3$ can be rewritten as

$$\begin{aligned} \mathcal{P}3\text{-1} : \quad & \max_{\mathbf{f}_c, \mathbf{w}_c, \mathbf{w}_s, \boldsymbol{\theta}} R(\mathbf{f}_c, \mathbf{w}_c, \boldsymbol{\theta}) \\ & s.t. \quad (52b), (52c), (52d). \end{aligned} \quad (55)$$

Since $R(\mathbf{f}_c, \mathbf{w}_c, \boldsymbol{\theta})$ monotonically increases w.r.t. $\frac{|\mathbf{w}_c^H \mathbf{H} \mathbf{f}_c|^2}{\sigma_c^2 \|\mathbf{w}_c^H\|^2}$, Problem $\mathcal{P}3\text{-1}$ is equivalent to

$$\begin{aligned} \mathcal{P}3\text{-2} : \quad & \max_{\mathbf{f}_c, \mathbf{w}_c, \mathbf{w}_s, \boldsymbol{\theta}} \frac{|\mathbf{w}_c^H \mathbf{H} \mathbf{f}_c|^2}{\sigma_c^2 \|\mathbf{w}_c^H\|^2} \\ & s.t. \quad (52b), (52c), (52d). \end{aligned} \quad (56)$$

Note that \mathbf{w}_s is only related to constraint (52c), while \mathbf{w}_c is related to the OF of Problem $\mathcal{P}3\text{-2}$. Therefore, the optimal solution for the decoding matrices \mathbf{w}_s and \mathbf{w}_c can be derived based on the maximum ratio combining (MRC) criterion as

$$\mathbf{w}_s^* = \arg \max \left(\frac{|\mathbf{w}_s^H \mathbf{G} \mathbf{f}_c|^2}{\|\mathbf{w}_s^H\|^2} \right) = \mathbf{G} \mathbf{f}_c, \quad (57)$$

$$\mathbf{w}_c^* = \arg \max \left(\frac{|\mathbf{w}_c^H \mathbf{H} \mathbf{f}_c|^2}{\|\mathbf{w}_c^H\|^2} \right) = \mathbf{H} \mathbf{f}_c. \quad (58)$$

By defining $\mathbf{h} = \frac{\mathbf{H}^H \mathbf{w}_c}{\sigma_c \|\mathbf{w}_c^H\|} \in \mathbb{C}^{N \times 1}$ and $\mathbf{g} = \frac{\mathbf{G}^H \mathbf{w}_s}{\sigma_s \|\mathbf{w}_s^H\|} \in \mathbb{C}^{N \times 1}$, the subproblem of optimizing \mathbf{f}_c can be formulated as follows:

$$\mathcal{P}3\text{-3} : \max_{\mathbf{f}_c} \left| \mathbf{h}^H \mathbf{f}_c \right|^2 \quad (59a)$$

$$s.t. \quad \|\mathbf{f}_c\|^2 \leq P_t, \quad (59b)$$

$$\left| \mathbf{g}^H \mathbf{f}_c \right|^2 \geq \eta. \quad (59c)$$

The following proposition contributes to addressing Problem $\mathcal{P}3\text{-3}$ [41], [42].

Proposition 2. *The optimal solution to Problem $\mathcal{P}3\text{-3}$ can be expressed as*

$$\mathbf{f}_c = a\mathbf{h} + b\mathbf{g}, \quad (60)$$

where $a, b \in \mathbb{C}$ are given as follows:

Case 1: If $\eta \leq \frac{P_t |\mathbf{g}^H \mathbf{h}|^2}{\|\mathbf{h}\|^2}$,

$$\begin{cases} |a| = \frac{\sqrt{P_t}}{\|\mathbf{h}\|}, \\ |b| = 0, \end{cases} \quad (61)$$

with an arbitrary phase shift.

Algorithm 5 Joint optimization of v , \mathbf{w}_c , \mathbf{w}_s , \mathbf{f}_c and $\boldsymbol{\theta}$

- 1: Initialize iteration number $t_5 = 0$. Set the maximum number of iterations to t_5^{\max} . Initialize feasible $\mathbf{f}_c^{(0)}$, $\mathbf{w}_c^{(0)}$, $\mathbf{w}_s^{(0)}$ and $\boldsymbol{\theta}^{(0)}$ following constraints (52b) - (52e).
- 2: **Repeat**
- 3: Calculate v by using (54)
- 4: Calculate $\mathbf{w}_c^{(t_5+1)}$ and $\mathbf{w}_s^{(t_5+1)}$ by using (57) and (58), respectively.
- 5: Calculate $\mathbf{f}_c^{(t_5+1)}$ following Proposition 2.
- 6: Calculate $\boldsymbol{\theta}^{(t_5+1)}$ by using (65).
- 7: $t_5 \leftarrow t_5 + 1$.
- 8: **Until** $t_5 = t_5^{\max}$ **or**

$$\epsilon_5^{(t_5+1)} = \frac{|\text{obj}^{(t_5+1)}(v, \mathbf{w}_c, \mathbf{f}_c, \boldsymbol{\theta}) - \text{obj}^{(t_5)}(v, \mathbf{w}_c, \mathbf{f}_c, \boldsymbol{\theta})|}{\text{obj}^{(t_5+1)}(v, \mathbf{w}_c, \mathbf{f}_c, \boldsymbol{\theta})} < \epsilon.$$

Case 2: If $\frac{P_t |\mathbf{g}^H \mathbf{h}|^2}{\|\mathbf{h}\|^2} \leq \eta \leq P_t \|\mathbf{g}\|^2$,

$$\begin{cases} |a| = \sqrt{\frac{P_t \|\mathbf{g}\|^2 - \eta}{\|\mathbf{h}\|^2 \|\mathbf{g}\|^2 - |\mathbf{h}^H \mathbf{g}|^2}}, \\ |b| = \frac{\sqrt{\eta}}{\|\mathbf{g}\|^2} - \frac{|\mathbf{h}^H \mathbf{g}|}{\|\mathbf{g}\|^2} |a|, \end{cases} \quad (62)$$

where the phase of a and b should satisfy

$$\angle(a) - \angle(b) = \angle(\mathbf{h}^H \mathbf{g}). \quad (63)$$

Case 3: If $\eta > P_t \|\mathbf{g}\|^2$, there exists no feasible solution.

Proof. Please refer to Appendix B. \square

Given $\{v, \mathbf{f}_c, \mathbf{w}_s, \mathbf{w}_c\}$, the following inequality holds for the OF of Problem $\mathcal{P}3\text{-2}$.

$$\frac{|\mathbf{w}_c^H (\mathbf{H}_{\text{bu}} + \mathbf{H}_r \mathbf{V} \mathbf{H}_{\text{ru}}) \mathbf{f}_c|^2}{\sigma_c^2 \|\mathbf{w}_c^H\|^2} \leq \frac{|\mathbf{w}_c^H \mathbf{H}_{\text{bu}} \mathbf{f}_c|^2}{\sigma_c^2 \|\mathbf{w}_c^H\|^2} + \frac{|\mathbf{w}_c^H \mathbf{H}_r \mathbf{V} \mathbf{H}_{\text{ru}} \mathbf{f}_c|^2}{\sigma_c^2 \|\mathbf{w}_c^H\|^2}. \quad (64)$$

Therefore, the optimal solution of $\boldsymbol{\theta}$ can be obtained via the following equation

$$\boldsymbol{\theta} = \angle(\mathbf{w}_c^H \mathbf{H}_{\text{bu}} \mathbf{f}_c) - \angle(\text{diag}\{\mathbf{w}_c^H \mathbf{H}_r\} \mathbf{H}_{\text{ru}} \mathbf{f}_c). \quad (65)$$

The overall algorithm for Problem $\mathcal{P}3$ is summarized in Algorithm 5. Next, we analyze the complexity of this algorithm. Note that the complexity of Algorithm 5 is dominated by Steps 4-6. Firstly, the complexities of using the MRC criterion to calculate $\mathbf{w}_c^{(t_5+1)}$ and $\mathbf{w}_s^{(t_5+1)}$ are on the order of $\mathcal{O}(N^2)$ and $\mathcal{O}(MN)$, respectively. Secondly, the complexity of calculating $\mathbf{f}_c^{(t_5+1)}$ following Proposition 2 is given by $\mathcal{O}(\max\{MN, N^2\})$. Finally, the complexity of calculating $\boldsymbol{\theta}^{(t_5+1)}$ by using (65) is $\mathcal{O}(L^2 N)$. Considering that $L \gg \{M, N\}$, the complexity of Algorithm 5 is on the order of $\mathcal{O}(L^2 N)$.

V. SIMULATION RESULTS

In this section, numerical results are provided to validate the performance of the proposed RIS-assisted ICSC system in both single-UE and multi-UE scenarios. As shown in Fig.

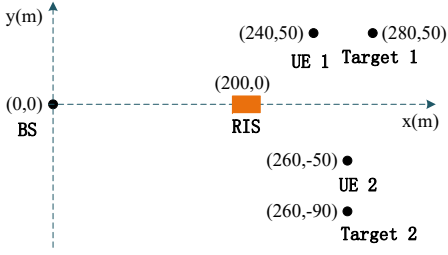


Fig. 2. The simulated multi-UE RIS-assisted ICSC scenario

2, the BS and the RIS are located at $(0, 0)$ and $(200 \text{ m}, 0)$, respectively. In the multi-UE scenario, we assume that two UEs are located at $(240 \text{ m}, 50 \text{ m})$ and $(260 \text{ m}, -50 \text{ m})$, with corresponding targets at $(280 \text{ m}, 50 \text{ m})$ and $(260 \text{ m}, -90 \text{ m})$, respectively. For the single-UE scenario, the UE is located at $(250 \text{ m}, 50 \text{ m})$ with its target at $(290 \text{ m}, 50 \text{ m})$.

In the context of wireless communication channels, we account for both small-scale fading and large-scale path loss. In specific, the large-scale path loss in dB is expressed as

$$PL = PL_0 - 10\alpha \log_{10} \left(\frac{d}{d_0} \right), \quad (66)$$

where PL_0 is the path loss at the reference distance d_0 , d represents the link distance and α denotes the corresponding path loss exponent. The path loss exponent of the UE-BS link, UE-RIS link, RIS-BS link, and UE-UE interference channel are denoted by α_{bu} , α_{ru} , and α_{r} , α_{uu} , respectively. The Rayleigh channel model is employed to characterize the communication channels between the BS and UEs, as well as the channels between UEs, due to the presence of potential scatters and obstacles. While the small-scale fading of channels associated with the RIS is assumed to follow a Rician fading distribution:

$$\tilde{\mathbf{H}} = \sqrt{\frac{K_R}{1+K_R}} \tilde{\mathbf{H}}_{\text{LoS}} + \sqrt{\frac{1}{1+K_R}} \tilde{\mathbf{H}}_{\text{NLoS}}, \quad (67)$$

where K_R is the Rician factor, $\tilde{\mathbf{H}}_{\text{LoS}}$ denotes the line of sight (LoS) component, and $\tilde{\mathbf{H}}_{\text{NLoS}}$ represents the non-line of sight (NLoS) component. The LoS component $\tilde{\mathbf{H}}_{\text{LoS}}$ is modeled as $\tilde{\mathbf{H}}_{\text{LoS}} = \mathbf{a}_r(\theta^{AoA}) \mathbf{a}_t^H(\theta^{AoD})$, where the steering vectors w.r.t. the angle of arrival (AoA) θ^{AoA} and the angle of departure (AoD) θ^{AoD} are given by

$$\begin{aligned} \mathbf{a}_r(\theta^{AoA}) &= [1, e^{j\frac{2\pi d}{\lambda} \sin \theta^{AoA}}, \dots, e^{j\frac{2\pi d}{\lambda} (D_r-1) \sin \theta^{AoA}}]^T, \\ \mathbf{a}_t(\theta^{AoD}) &= [1, e^{j\frac{2\pi d}{\lambda} \sin \theta^{AoD}}, \dots, e^{j\frac{2\pi d}{\lambda} (D_t-1) \sin \theta^{AoD}}]^T. \end{aligned} \quad (68)$$

In (68), D_r and D_t represent the numbers of antennas at the receiver side and the transmitter side, respectively, and parameters d and λ denote the antenna spacing and wavelength, respectively. For simplicity, we set $d/\lambda = 1/2$. The detailed settings of the above parameters are specified in the ‘‘Communication and Radar model’’ block and the computing parameters V_k , c_k , f_k^l and f_{total}^e are specified in the ‘‘Computation model’’ block of Table I.

In the subsequent subsections, we evaluate our proposed algorithms against the benchmark schemes listed below:

- **RandPhase:** Assuming that the RIS phase shifts are randomly generated following a uniform distribution from 0

TABLE I
DEFAULT SIMULATION PARAMETER SETTINGS

Description	Parameter and Value
Communication and Radar model	$PL_0 = 30 \text{ dB}$, $d_0 = 1 \text{ m}$ $\alpha_{\text{bu}} = 3.75$, $\alpha_{\text{r}} = 2.2$, $\alpha_{\text{ru}} = 2.2$ $\alpha_{\text{uu}} = 2.2$, $B_\omega = 1 \text{ MHz}$ $M = 4$, $N = 2$, $d = 2$ $P_{t,k}^{\text{max}} = 10 \text{ mW}$, $\eta = 10 \text{ dB}$ $K_R = 3$, $L = 30$ $\sigma_s^2 = 3.98 \times 10^{-12} \text{ mW}$ $\sigma_s^2 = 3.98 \times 10^{-12} \text{ mW}$
Computation model	$V_k = [200, 300] \text{ Kb}$ $c_k = [500, 600] \text{ cycle/bit}$ $f_k^l = [1 \times 10^8, 2 \times 10^8] \text{ cycle/s}$ $f_{\text{total}}^e = 5 \times 10^9 \text{ cycle/s}$
Weight	$\xi_k = 1/K$
Convergence criterion	$\epsilon = 10^{-3}$

to 2π , we jointly optimize the precoding and decoding matrices of UEs, the offloading volume, and the edge computational resource allocation. This optimization is conducted according to Algorithm 5 and Algorithm 4 in the single-UE and multi-UE scenarios, respectively, while excluding the design of the RIS phase shift.

- **Without RIS:** The RIS-UE links are assumed to be blocked. Only the precoding and decoding matrices of UEs, along with the offloading volume and the edge computational resource allocation, are jointly optimized using Algorithm 5 and Algorithm 4 in the single-UE and multi-UE scenarios, respectively.

Fig. 3 presents the weighted latency versus the number of iterations for various numbers of RIS reflecting elements, i.e. $L = 10$, $L = 30$, and $L = 50$, in both single-UE and multi-UE scenarios. It can be seen from Fig. 3 that as the number of reflecting elements increases, the latency decreases due to the strengthened RIS-related link. Furthermore, both the proposed algorithms demonstrate rapid convergence within 5 iterations.

Fig. 4 illustrates the algorithm performance under different initialization settings in both single-UE and multi-UE scenarios. We consider 10 channel realizations and parameters for random computational tasks, labeled 1-10. For each specific generation of channels and computational tasks, we randomly initialize the optimization variables 100 times and subsequently calculate the corresponding solutions using the algorithm outlined in the preceding section. Within these 100 result sets, the maximum latency, denoted by **Max**, represents the worst solution obtained from the algorithm, while the minimum latency, approximating the global optimal value, is designated as **Min**, as depicted in Fig. 4. Notably, in the single-UE scenario, the values of **Max** and **Min** are similar, suggesting a high probability of achieving the globally optimal solution. In the multi-UE scenario, the maximum deviation is 12%, indicating that the solutions generated by the proposed algorithm closely approach the optimal solution.

Fig. 5 depicts the weighted latency versus the number of RIS elements. In addition to the three aforementioned benchmark schemes, we also explore two scenarios where the continuous RIS phase shifts are quantized to 1 and 2 bits due to the practical hardware constraints. Specifically, in the **With RIS**,

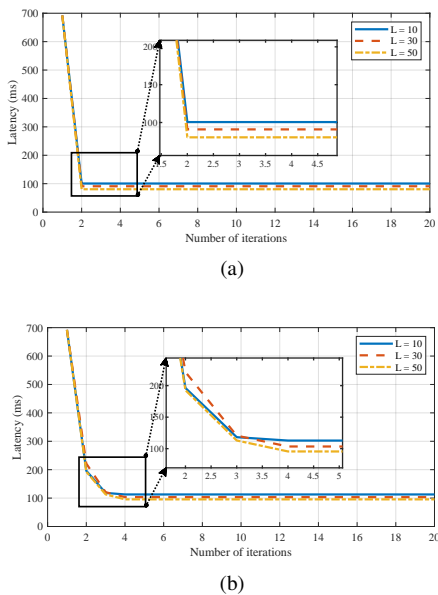


Fig. 3. Convergence behavior of the proposed algorithm for (a) the single-UE scenario using Algorithm 5 and (b) the multi-UE scenario using Algorithm 4.

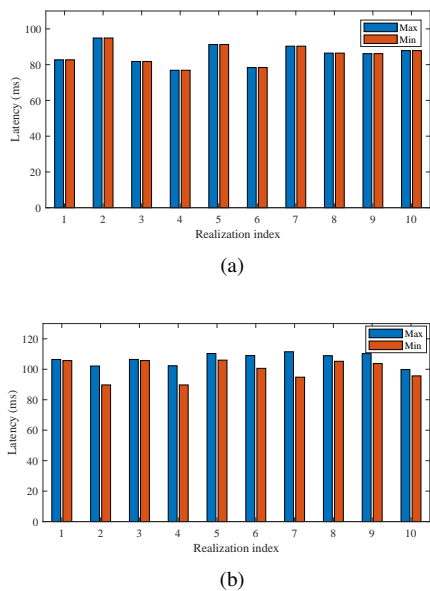


Fig. 4. Simulation results of the maximum and minimum latency versus the realization index obtained under 100 random initialization settings for (a) the single-UE scenario using Algorithm 5 and (b) the multi-UE scenario using Algorithm 4.

1 bit scheme, the phase shift of RIS elements is limited to either 0 or π , whereas the **With RIS, 2 bit** scheme offers four options: $\{0, \frac{\pi}{2}, \pi, \frac{3\pi}{2}\}$. Our observations yield the following insights. Firstly, the latency of the **RandPhase** scheme exhibits a gradual decrease w.r.t. the number of RIS elements, widening the gap with the **Without RIS** scheme. This suggests that integrating RIS can enhance communication performance even in the absence of intricate phase shift designs for the RIS elements. Secondly, the performance improvement of the **With RIS** scheme over the **RandPhase** scheme is observed to amplify with the increase of RIS elements. This observation underscores the significance of meticulously designing

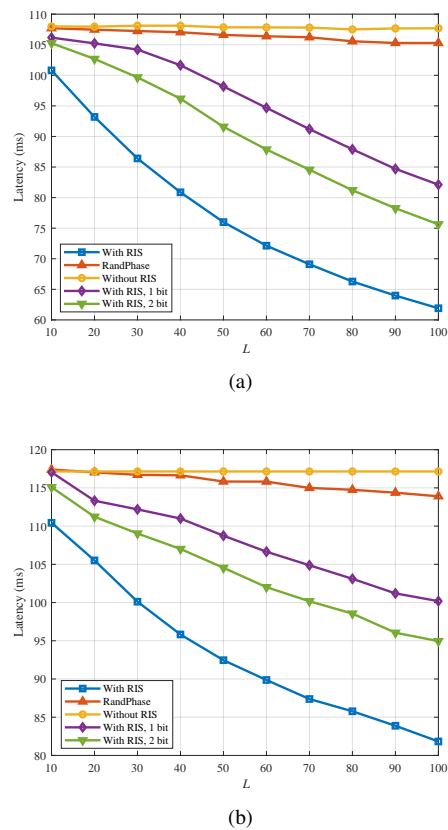
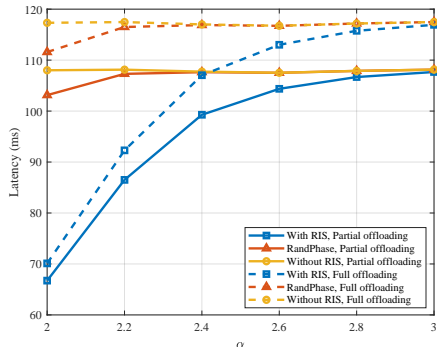


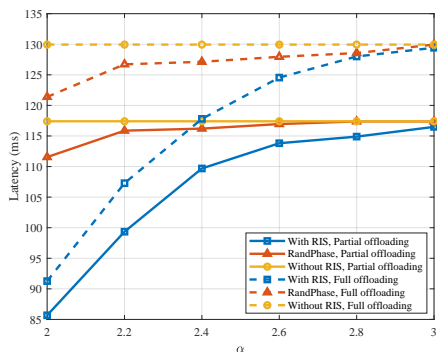
Fig. 5. Latency versus the number of RIS elements for (a) the single-UE scenario using Algorithm 5 and (b) the multi-UE scenario using Algorithm 4.

the phase-shift response of RIS for enhancing beamforming gain with an increasing number of RIS elements. Finally, in comparison to the **With RIS, 1 bit** scheme, the latency in the **With RIS, 2 bit** scheme is reduced and approaches the levels observed in the continuous phase shift scheme **With RIS**. This finding suggests that considering continuous phase design can serve as a tight bound for evaluating the practical discrete RIS phase shift configuration.

Fig. 6 plots the weighted latency versus the path loss exponent associated with RIS under different offloading strategies. It can be seen from Fig. 6 that as expected, the latency escalates w.r.t. α_{RIS} . In addition, the latency in the **RandPhase** scheme closely resembles that of the **Without RIS** scheme when the value of α_{RIS} is substantial. This is because the beamforming gain introduced by the RIS cannot compensate for an increasing channel path-loss α_{RIS} and the direct UE-BS links are dominated. This implies that in practical applications, strategic placement of the RIS is crucial to circumvent obstacles and achieve reduced values of α_r and α_{ru} . Additionally, we examine the influence of offloading strategies. The latency achieved with the partial offloading strategy is smaller than that with the full offloading strategy, and the disparity between the two strategies is widened as α_r increases. The reason for this discrepancy can be explained as follows. In scenarios with favorable channel conditions, both strategies tend to offload the computational task to the edge server. However, as the RIS-related channel deteriorates, the partial offloading strategy



(a)



(b)

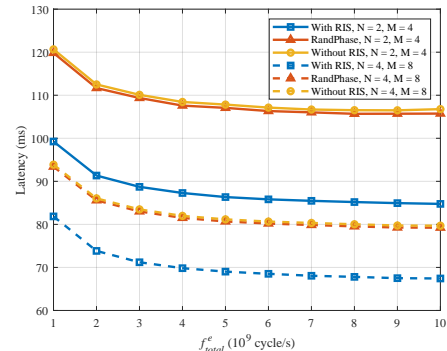
Fig. 6. Latency versus the α_{RIS} path loss exponent for (a) the single-UE scenario using Algorithm 5 and (b) the multi-UE scenario using Algorithm 4.

becomes smarter in the processing part of the computational task locally.

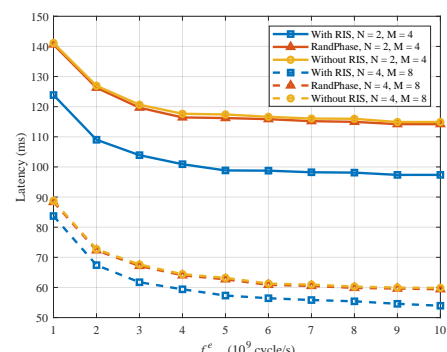
Fig. 7 shows the weighted latency versus the edge computing capability under different numbers of transmit and receive antennas. The latency initially decreases significantly as the processing rate of the ECS f_{total}^e rises, followed by a deceleration in the rate of latency reduction. This is because at lower f_{total}^e values, the latency is primarily influenced by edge computing capability. By contrast, at higher f_{total}^e levels, the computation offloading delay is dominant in the overall latency. As a result, minimizing latency does not necessarily require equipping edge computing nodes with excessively powerful computational capabilities. Furthermore, a noteworthy decrease in latency occurs with an increase in the numbers of transmit and receive antennas, especially in the multi-UE scenario.

VI. CONCLUSION

In this paper, we conducted an investigation into RIS-assisted ICSC systems to enhance the performance of DFRC-enabled UEs. A latency minimization problem was formulated by jointly optimizing the precoding and decoding matrices of the uplink signal, the receive radar beamforming vector, the RIS phase shift vector, the offloading volume, and the edge computational resource allocation. To address the non-convexity of the problem, we proposed an algorithm based on the BCD method to optimize the computational and beam-



(a)



(b)

Fig. 7. Latency versus the edge computing capability for (a) the single-UE scenario using Algorithm 5 and (b) the multi-UE scenario using Algorithm 4.

forming settings alternately. Specifically, we employed the Lagrangian method for the optimization of computational settings. In addition, two equivalent transformations were applied to transform the OF of the subproblem for active and passive beamforming into a form of weighted sum-rate, which was tackled by using a pair of efficient algorithms. Moreover, a low complexity algorithm with closed-form solutions is provided in the simplified systems. Simulation results indicated a significant performance enhancement in latency with the proposed algorithm compared to the conventional approach operating without the integration of an RIS, quantitatively from 100 ms to 117 ms in a two-UE ICSC system. Furthermore, numerical analysis confirmed the efficiency of our proposed algorithm.

APPENDIX A

THE PROOF OF PROPOSITION 1

The partial Lagrange function of Problem $\mathcal{P}2$ -1 is given by

$$\mathcal{L}(\mathbf{F}_c, \mathbf{W}_c, \boldsymbol{\theta}, \boldsymbol{\lambda}) = \sum_{k=1}^K \lambda_k + \sum_{k=1}^K \delta_k [\xi_k v_k - \lambda_k R_k(\mathbf{F}_c, \mathbf{W}_c, \boldsymbol{\theta})], \quad (\text{A.1})$$

where $\{\delta_k\}$ is the Lagrange multiplier. Given that $\{\mathbf{F}_c^*, \mathbf{W}_c^*, \mathbf{w}_s^*, \boldsymbol{\theta}^*, \boldsymbol{\lambda}^*\}$ represents the solution to Problem $\mathcal{P}2$ -1, there exists $\boldsymbol{\delta}^*$ that fulfills the following KKT conditions:

$$\frac{\partial \mathcal{L}}{\partial \theta_k} = -\delta_k^* \lambda_k^* \nabla R_k(\mathbf{F}_c^*, \mathbf{W}_c^*, \boldsymbol{\theta}^*) = 0, \forall k \in \mathcal{K}, \quad (\text{A.2})$$

$$\frac{\partial \mathcal{L}}{\partial \mathbf{F}_{c,k}} = -\delta_k^* \lambda_k^* \nabla R_k(\mathbf{F}_c^*, \mathbf{W}_c^*, \boldsymbol{\theta}^*) = 0, \forall k \in \mathcal{K}, \quad (\text{A.3})$$

$$\frac{\partial \mathcal{L}}{\partial \mathbf{W}_{c,k}} = -\delta_k^* \lambda_k^* \nabla R_k(\mathbf{F}_c^*, \mathbf{W}_c^*, \boldsymbol{\theta}^*) = 0, \forall k \in \mathcal{K}, \quad (\text{A.4})$$

$$\frac{\partial \mathcal{L}}{\partial \lambda_k} = 1 - \delta_k^* R_k(\mathbf{F}_c^*, \mathbf{W}_c^*, \boldsymbol{\theta}^*) = 0, \forall k \in \mathcal{K}, \quad (\text{A.5})$$

$$\delta_k^* [\xi_k v_k - \lambda_k^* R_k(\mathbf{F}_c^*, \mathbf{W}_c^*, \boldsymbol{\theta}^*)] = 0, \forall k \in \mathcal{K}, \quad (\text{A.6})$$

$$\delta_k^* \geq 0, \forall k \in \mathcal{K}, \quad (\text{A.7})$$

$$\xi_k v_k - \lambda_k^* R_k(\mathbf{F}_c^*, \mathbf{W}_c^*, \boldsymbol{\theta}^*) \leq 0, \forall k \in \mathcal{K}, \quad (\text{A.8})$$

$$0 \leq \theta_k^* \leq 2\pi, \forall k \in \mathcal{K}. \quad (\text{A.9})$$

Since $R_k(\mathbf{F}_c, \boldsymbol{\theta}) > 0$, (A.5) is equivalent to

$$\delta_k^* = \frac{1}{R_k(\mathbf{F}_c^*, \mathbf{W}_c^*, \boldsymbol{\theta}^*)}, \forall k \in \mathcal{K}. \quad (\text{A.10})$$

From (A.6), we can derive that

$$\lambda_k^* = \frac{\xi_k v_k}{R_k(\mathbf{F}_c^*, \mathbf{W}_c^*, \boldsymbol{\theta}^*)}, \forall k \in \mathcal{K}. \quad (\text{A.11})$$

When we set $\boldsymbol{\lambda} = \boldsymbol{\lambda}^*$ and $\boldsymbol{\delta} = \boldsymbol{\delta}^*$, the KKT conditions of Problem $\mathcal{P}2$ -2 are the same as (A.2), (A.3), (A.4), and (A.9). Thus, Proposition 1 is proved.

APPENDIX B THE PROOF OF PROPOSITION 2

First, we demonstrate that when the OF of Problem $\mathcal{P}3$ -3 is maximized, the constraint in (59b) achieves the upper bound $\mathbf{f}_c \mathbf{f}_c^H = P_t$ by using the proof by contradiction. Assuming that \mathbf{f}_c^* represents the optimal solution of Problem $\mathcal{P}3$ -3 such that $\mathbf{f}_c^* \mathbf{f}_c^{*H} < P_t$, we can derive $\hat{\mathbf{f}}_c = (1 + \beta) \mathbf{f}_c^*$ satisfying $\hat{\mathbf{f}}_c \hat{\mathbf{f}}_c^H = P_t$, where $\beta \geq 0$, as a feasible solution of Problem $\mathcal{P}3$ -3. Since the OF of Problem $\mathcal{P}3$ -3 when $\mathbf{f}_c = \hat{\mathbf{f}}_c$ surpasses that when $\mathbf{f}_c = \mathbf{f}_c^*$, the OF of Problem $\mathcal{P}3$ -3 is maximized if and only if when $\mathbf{f}_c \mathbf{f}_c^H = P_t$. Thus, Problem $\mathcal{P}3$ -3 can be rewritten as

$$\max_{\mathbf{f}_c} \quad \left| \mathbf{h}^H \mathbf{f}_c \right|^2 \quad (\text{B.1a})$$

$$s.t. \quad \left| \mathbf{f}_c \right|^2 = P_t, \quad (\text{B.1b})$$

$$\left| \mathbf{g}^H \mathbf{f}_c \right|^2 \geq \eta. \quad (\text{B.1c})$$

If $\eta > P_t \|\mathbf{g}\|^2$, by applying the Cauchy's inequality, we have $|\mathbf{g}^H \mathbf{f}_c|^2 \leq \|\mathbf{g}\|^2 \|\mathbf{f}_c\|^2 = P_t \|\mathbf{g}\|^2 < \eta$, which is in conflict with constraint (B.1c). Thus, Problem (B.1) is feasible only when $\eta \leq P_t \|\mathbf{g}\|^2$. Case 3 in Proposition 2 is proved.

As Problem (B.1) is convex and satisfies Slater's condition [33], the KKT conditions are utilized to address this problem. The Lagrange function of Problem (B.1) is expressed as

$$\mathcal{L}(\mathbf{f}_c) = -\mathbf{h}^H \mathbf{f}_c \mathbf{f}_c^H \mathbf{h} + \varphi(\eta - \mathbf{g}^H \mathbf{f}_c \mathbf{f}_c^H \mathbf{g}) + \iota(\mathbf{f}_c \mathbf{f}_c^H - P_t), \quad (\text{B.2})$$

where φ and ι are the Lagrange multipliers. Then, the KKT conditions for (B.1) can be formulated as follows:

$$\frac{\partial \mathcal{L}}{\partial \mathbf{f}_c^*} = -\mathbf{h}^H \mathbf{f}_c \mathbf{h} - \varphi \mathbf{g}^H \mathbf{f}_c \mathbf{g} + \iota \mathbf{f}_c = \mathbf{0}, \quad (\text{B.3})$$

$$\eta - \mathbf{g}^H \mathbf{f}_c \mathbf{f}_c^H \mathbf{g} \leq 0, \quad (\text{B.4})$$

$$\mathbf{f}_c \mathbf{f}_c^H - P_t = 0, \quad (\text{B.5})$$

$$\varphi \geq 0, \quad (\text{B.6})$$

$$\varphi(\eta - \mathbf{g}^H \mathbf{f}_c \mathbf{f}_c^H \mathbf{g}) = 0. \quad (\text{B.7})$$

(B.3) is equivalent to

$$\mathbf{f}_c = \frac{\mathbf{h}^H \mathbf{f}_c}{\iota} \mathbf{h} + \frac{\varphi \mathbf{g}^H \mathbf{f}_c}{\iota} \mathbf{g}, \quad (\text{B.8})$$

which indicates $\mathbf{f}_c \in \text{span}(\mathbf{h}, \mathbf{g})$. For convenience, \mathbf{f}_c can be rewritten as

$$\mathbf{f}_c = a\mathbf{h} + b\mathbf{g}, \quad (\text{B.9})$$

where a and b are the coefficients. By substituting (B.9) into (B.5), we obtain that

$$|a|^2 \mathbf{h}^H \mathbf{h} + a^* b \mathbf{h}^H \mathbf{g} + ab^* \mathbf{g}^H \mathbf{h} + |b|^2 \mathbf{g}^H \mathbf{g} = P_t. \quad (\text{B.10})$$

Moreover, (B.7) suggests that either φ or $\eta - \mathbf{g}^H \mathbf{f}_c \mathbf{f}_c^H \mathbf{g}$ equals to 0. Next, we discuss the different cases separately.

1) When $\varphi = 0$, (B.8) is transformed into

$$\mathbf{f}_c = \frac{\mathbf{h}^H \mathbf{f}_c}{\iota} \mathbf{h}. \quad (\text{B.11})$$

By substituting (B.9) into (B.11), we derive that

$$a\mathbf{h} + b\mathbf{g} = \frac{a\mathbf{h}^H \mathbf{h} + b\mathbf{h}^H \mathbf{g}}{\iota} \mathbf{h}. \quad (\text{B.12})$$

From (B.12), it can be deduced that $b = 0$. By substituting $b = 0$ into (B.10), the value of a can be determined as

$$|a| = \frac{\sqrt{P_t}}{\|\mathbf{h}\|}, \quad (\text{B.13})$$

where the phase of a is arbitrary. Meanwhile, it can be derived from (B.4) that

$$\eta \leq \frac{P_t |\mathbf{g}^H \mathbf{h}|^2}{\|\mathbf{h}\|^2}. \quad (\text{B.14})$$

Thus, Case 1 in Proposition 2 is proved.

2) When $\eta - \mathbf{g}^H \mathbf{f}_c \mathbf{f}_c^H \mathbf{g} = 0$, by substituting (B.9) into $\eta - \mathbf{g}^H \mathbf{f}_c \mathbf{f}_c^H \mathbf{g} = 0$ and (B.8), we have

$$|a|^2 \mathbf{g}^H \mathbf{h} \mathbf{h}^H \mathbf{g} + a^* b \mathbf{g}^H \mathbf{g} \mathbf{h}^H \mathbf{g} + ab^* \mathbf{g}^H \mathbf{h} \mathbf{g}^H \mathbf{g} + |b|^2 \mathbf{g}^H \mathbf{g} \mathbf{g}^H \mathbf{g} = \eta, \quad (\text{B.15})$$

$$a\mathbf{h} + b\mathbf{g} = \frac{a\mathbf{h}^H \mathbf{h} + b\mathbf{h}^H \mathbf{g}}{\iota} \mathbf{h} + \frac{\varphi(a\mathbf{g}^H \mathbf{h} + b\mathbf{g}^H \mathbf{g})}{\iota} \mathbf{g}. \quad (\text{B.16})$$

From (B.10) and (B.15), it can be derived that

$$|a| = \sqrt{\frac{P_t \|\mathbf{g}\|^2 - \eta}{\|\mathbf{h}\|^2 \|\mathbf{g}\|^2 - |\mathbf{h}^H \mathbf{g}|^2}}. \quad (\text{B.17})$$

From (B.16), we obtain that

$$\angle(a) = \angle(a\mathbf{h}^H \mathbf{h} + b\mathbf{h}^H \mathbf{g}) = \angle(b\mathbf{h}^H \mathbf{g}), \quad (\text{B.18})$$

$$\angle(b) = \angle(a\mathbf{g}^H \mathbf{h} + b\mathbf{g}^H \mathbf{g}) = \angle(a\mathbf{g}^H \mathbf{h}). \quad (\text{B.19})$$

It follows

$$\angle(a) - \angle(b) = \angle(\mathbf{h}^H \mathbf{g}). \quad (\text{B.20})$$

Meanwhile, by substituting (B.17) and (B.20) into (B.10), we derive that

$$|b| = \frac{\sqrt{\eta}}{\|\mathbf{g}\|^2} - \frac{|\mathbf{h}^H \mathbf{g}|}{\|\mathbf{g}\|^2} |a|. \quad (\text{B.21})$$

Furthermore, since $|b| \geq 0$, the parameter η satisfies $\eta \geq \frac{P_t |\mathbf{g}^H \mathbf{h}|^2}{\|\mathbf{h}\|^2}$. Thus, Case 2 in Proposition 2 is proved.

REFERENCES

- [1] D. K. Pin Tan, J. He, Y. Li, A. Bayesteh, Y. Chen, P. Zhu, and W. Tong, "Integrated sensing and communication in 6G: Motivations, use cases, requirements, challenges and future directions," in *Proc. 2021 1st IEEE Int. Online Symp. Joint Commun. & Sensing (JC&S)*, Feb. 2021, pp. 1–6.
- [2] A. Liu, Z. Huang, M. Li, Y. Wan, W. Li, T. X. Han, C. Liu, R. Du, D. K. P. Tan, J. Lu, Y. Shen, F. Colone, and K. Chetty, "A survey on fundamental limits of integrated sensing and communication," *IEEE Commun. Surv. Tuts.*, vol. 24, no. 2, pp. 994–1034, Feb. 2022.
- [3] R. Liu, M. Li, Y. Liu, Q. Wu, and Q. Liu, "Joint transmit waveform and passive beamforming design for RIS-aided DFRC systems," *IEEE J. Sel. Top. in Signal Process.*, vol. 16, no. 5, pp. 995–1010, May 2022.
- [4] A. Hassanien, M. G. Amin, Y. D. Zhang, and F. Ahmad, "Dual-function radar-communications: Information embedding using sidelobe control and waveform diversity," *IEEE Trans. Signal Process.*, vol. 64, no. 8, pp. 2168–2181, Dec. 2016.
- [5] B. Paul, A. R. Chiriyath, and D. W. Bliss, "Survey of RF communications and sensing convergence research," *IEEE Access*, vol. 5, pp. 252–270, Dec. 2017.
- [6] L. Zheng, M. Lops, Y. C. Eldar, and X. Wang, "Radar and communication coexistence: An overview: A review of recent methods," *IEEE Signal Process. Mag.*, vol. 36, no. 5, pp. 85–99, Sep. 2019.
- [7] A. Hassanien, M. G. Amin, E. Aboutanos, and B. Himed, "Dual-function radar communication systems: A solution to the spectrum congestion problem," *IEEE Signal Process. Mag.*, vol. 36, no. 5, pp. 115–126, Sep. 2019.
- [8] N. Q. Hieu, D. T. Hoang, N. C. Luong, and D. Niyato, "iRDRC: An intelligent real-time dual-functional radar-communication system for automotive vehicles," *IEEE Wireless Commun. Lett.*, vol. 9, no. 12, pp. 2140–2143, Aug. 2020.
- [9] S. Bi and Y. Zhang, "Computation rate maximization for wireless powered mobile-edge computing with binary computation offloading," *IEEE Trans. Wireless Commun.*, vol. 17, no. 6, pp. 4177–4190, Jun. 2018.
- [10] Z. Wang, Y. Wei, Z. Feng, F. R. Yu, and Z. Han, "Resource management and reflection optimization for intelligent reflecting surface assisted multi-access edge computing using deep reinforcement learning," *IEEE Trans. Wireless Commun.*, vol. 22, no. 2, pp. 1175–1186, Feb. 2023.
- [11] D. Wen, P. Liu, G. Zhu, Y. Shi, J. Xu, Y. C. Eldar, and S. Cui, "Task-oriented sensing, computation, and communication integration for multi-device edge AI," *IEEE Trans. Wireless Commun.*, pp. 1–1, Aug. 2023.
- [12] J. A. Zhang, M. L. Rahman, K. Wu, X. Huang, Y. J. Guo, S. Chen, and J. Yuan, "Enabling joint communication and radar sensing in mobile networks—a survey," *IEEE Commun. Surv. Tuts.*, vol. 24, no. 1, pp. 306–345, Oct. 2022.
- [13] X. Chen, Z. Feng, J. A. Zhang, Z. Yang, X. Yuan, X. He, and P. Zhang, "Integrated communication, sensing, and computation framework for 6G networks," 2023, [Online]. Available: <https://arxiv.org/abs/2310.03265>.
- [14] X. Li, F. Liu, Z. Zhou, G. Zhu, S. Wang, K. Huang, and Y. Gong, "Integrated sensing, communication, and computation over-the-air: MIMO beamforming design," *IEEE Trans. Wireless Commun.*, vol. 22, no. 8, pp. 5383–5398, Aug. 2023.
- [15] Y. He, G. Yu, Y. Cai, and H. Luo, "Integrated sensing, computation, and communication: System framework and performance optimization," *IEEE Trans. Wireless Commun.*, pp. 1–1, Jun. 2023.
- [16] Q. Liu, R. Luo, H. Liang, and Q. Liu, "Energy-efficient joint computation offloading and resource allocation strategy for ISAC-aided 6G V2X networks," *IEEE Trans. Green Commun. Netw.*, vol. 7, no. 1, pp. 413–423, Jan. 2023.
- [17] N. Huang, C. Dou, Y. Wu, L. Qian, B. Lin, and H. Zhou, "Unmanned-aerial-vehicle-aided integrated sensing and computation with mobile-edge computing," *IEEE Internet Things J.*, vol. 10, no. 19, pp. 16830–16844, Apr. 2023.
- [18] P. Rajput, L. Wu, and M. R. Bhavani Shankar, "Next-generation IoT networks: Integrated sensing communication and computation," in *Proc. 2023 IEEE Int. Conf. Acoust. Speech Signal Process. Workshops (ICASSP)*, Jun. 2023, pp. 1–4.
- [19] N. Huang, C. Dou, Y. Wu, L. Qian, and R. Lu, "Energy-efficient integrated sensing and communication: A multi-access edge computing design," *IEEE Wireless Commun. Lett.*, pp. 1–1, Aug. 2023.
- [20] C. Ding, J. Wang, H. Zhang, M. Lin, and G. Y. Li, "Joint MIMO precoding and computation resource allocation for dual-function radar and communication systems with mobile edge computing," *IEEE J. Sel. Areas Commun.*, vol. 40, no. 7, pp. 2085–2102, Mar. 2022.
- [21] Z. Peng, R. Weng, Z. Zhang, C. Pan, and J. Wang, "Active reconfigurable intelligent surface for mobile edge computing," *IEEE Wireless Commun. Lett.*, vol. 11, no. 12, pp. 2482–2486, Sep. 2022.
- [22] K. Zhi, C. Pan, H. Ren, K. Chai, and M. ElKashlan, "Active RIS versus passive RIS: Which is superior with the same power budget?" *IEEE Commun. Lett.*, vol. 26, no. 5, pp. 1150–1154, May 2022.
- [23] C. Pan, G. Zhou, K. Zhi, S. Hong, T. Wu, Y. Pan, H. Ren, M. D. Renzo, A. Lee S., R. Zhang, and A. Y. Zhang, "An overview of signal processing techniques for RIS/IRS-aided wireless systems," *IEEE J. Sel. Top. Signal Process.*, vol. 16, no. 5, pp. 883–917, Aug. 2022.
- [24] T. Bai, C. Pan, Y. Deng, M. ElKashlan, A. Nallanathan, and L. Hanzo, "Latency minimization for intelligent reflecting surface aided mobile edge computing," *IEEE J. Sel. Areas Commun.*, vol. 38, no. 11, pp. 2666–2682, Jul. 2020.
- [25] A. Huang, L. Qu, and M. J. Khabbaz, "Latency-aware computation offloading in multi-RIS-assisted edge networks," *IEEE Open Journal of the Communications Society*, vol. 5, pp. 1204–1221, Feb. 2024.
- [26] M. Mukherjee, V. Kumar, S. Kumar, C. X. Mavromoustakis, Q. Zhang, and M. Guo, "RIS-assisted task offloading for wireless dead zone to minimize delay in edge computing," in *Proc. 2022 IEEE Global Commun. Conf. (GLOBECOM)*, Dec. 2022, pp. 2554–2559.
- [27] Z. Jiang, M. Rihan, P. Zhang, L. Huang, Q. Deng, J. Zhang, and E. M. Mohamed, "Intelligent reflecting surface aided dual-function radar and communication system," *IEEE Syst. J.*, vol. 16, no. 1, pp. 475–486, Mar. 2022.
- [28] Z. Yu, H. Ren, C. Pan, G. Zhou, B. Wang, M. Dong, and J. Wang, "Active RIS aided ISAC systems: Beamforming design and performance analysis," *IEEE Trans. Commun.*, pp. 1–1, Nov. 2023.
- [29] N. Huang, T. Wang, Y. Wu, Q. Wu, and T. Q. S. Quek, "Integrated sensing and communication assisted mobile edge computing: An energy-efficient design via intelligent reflecting surface," *IEEE Wireless Commun. Lett.*, vol. 11, no. 10, pp. 2085–2089, Jul. 2022.
- [30] S. Xu, Y. Du, J. Zhang, J. Liu, J. Wang, and J. Zhang, "Intelligent reflecting surface enabled integrated sensing, communication and computation," *IEEE Trans. Wireless Commun.*, pp. 1–1, Jul. 2023.
- [31] R. P. Sankar, S. P. Chepuri, and Y. C. Eldar, "Beamforming in integrated sensing and communication systems with reconfigurable intelligent surfaces," *IEEE Trans. Wireless Commun.*, pp. 1–1, Sep. 2023.
- [32] M. Bennis, M. Debbah, and H. V. Poor, "Ultrareliable and low-latency wireless communication: Tail, risk, and scale," *Proc. IEEE*, vol. 106, no. 10, pp. 1834–1853, Oct. 2018.
- [33] S. Boyd and L. Vandenberghe, *Convex Optimization*. Cambridge, U.K.: Cambridge Univ. Press, 2004.
- [34] C. Pan, H. Ren, K. Wang, M. ElKashlan, A. Nallanathan, J. Wang, and L. Hanzo, "Intelligent reflecting surface aided MIMO broadcasting for simultaneous wireless information and power transfer," *IEEE J. Sel. Areas Commun.*, vol. 38, no. 8, pp. 1719–1734, Aug. 2020.
- [35] Y. Jong, "An efficient global optimization algorithm for nonlinear sum-of-ratios problem," *Optimization Online*, pp. 1–21, 2012.
- [36] Q. Shi, M. Razaviyayn, Z. Luo, and C. He, "An iteratively weighted MMSE approach to distributed sum-utility maximization for a MIMO interfering broadcast channel," in *Proc. 2011 IEEE Int. Conf. Acoust. Speech Signal Process. (ICASSP)*, Jul. 2011, pp. 3060–3063.
- [37] J. Capon, "High-resolution frequency-wavenumber spectrum analysis," *Proc. IEEE Inst. Electr. Electron. Eng.*, vol. 57, no. 8, pp. 1408–1418, Aug. 1969.
- [38] M. Grant and S. Boyd, "CVX: Matlab software for disciplined convex programming, version 2.1," 2014.
- [39] Y. Sun, P. Babu, and P. Palomar, "Majorization-minimization algorithms in signal processing, communications, and machine learning," *IEEE Trans. Signal Process.*, vol. 65, no. 3, pp. 794–816, Feb. 2017.
- [40] C. Pan, H. Ren, K. Wang, W. Xu, M. ElKashlan, A. Nallanathan, and L. Hanzo, "Multicell MIMO communications relying on intelligent reflecting surfaces," *IEEE Trans. Wireless Commun.*, vol. 19, no. 8, pp. 5218–5233, Aug. 2020.
- [41] A. Bazzi and M. Chafii, "On outage-based beamforming design for dual-functional radar-communication 6G systems," *IEEE Trans. Wireless Commun.*, vol. 22, no. 8, pp. 5598–5612, Aug. 2023.
- [42] Z. Zheng, X. Liu, T. Huang, Y. Liu, and Y. Eldar, "Towards a performance bound on MIMO DFRC systems," 2022, [Online]. Available: <https://arxiv.org/abs/2211.06979>.